Human birth tissue products as a regenerative medicine to inhibit post-surgical pain through multi-modal action

Chi Zhang[1*], Qian Huang[1*], Neil C. Ford[1*], Nathachit Limjunyawong[2], Qing Lin[1], Fei Yang[1], Xiang Cui[1], Ankit Uniyal[1], Jing Liu[1], Megha Mahabole[3], Hua He[3], Xue-Wei Wang[1,4], Irina Duff[1], Yiru Wang[1], Jieru Wan[1], Guangwu Zhu[1], Srinivasa N Raja[1], Hongpeng Jia[6], Dazhi Yang[7], Xinzhong Dong[2,5], Scheffer C. Tseng[3], Shao-Qiu He[1#], Yun Guan[1,8 #]

[1] Department of Anesthesiology and Critical Care Medicine, Johns Hopkins University, School of Medicine, Baltimore, Maryland, 21205, USA.

[2] The Solomon H. Snyder Department of Neuroscience, Center for Sensory Biology, Johns Hopkins University, School of Medicine, Baltimore, Maryland, 21205, USA.

[3] BioTissue, Inc., Miami, Florida, USA.

[4] Department of Orthopedics, Johns Hopkins University, School of Medicine, Baltimore, Maryland, 21205, USA.

[5] Howard Hughes Medical Institute, Johns Hopkins University, School of Medicine, Baltimore, Maryland, 21205, USA.

[6] Department of Surgery, Johns Hopkins University, School of Medicine, Baltimore, Maryland, 21205, USA.

[7] Acrogenic Technologies Inc., Rockville, Maryland, 20847, USA.

[8] Department of Neurological Surgery, Johns Hopkins University, School of Medicine, Baltimore, Maryland, 21205, USA.

[*]These authors contributed equally to this work.

Corresponding authors:

Yun Guan, MD, PhD, Department of Anesthesiology and Critical Care Medicine, Johns Hopkins University, School of Medicine, Baltimore, MD, 21205, USA. Phone: 410-614-2909; Fax: 410-614-2909; E-mail: yguan1@jhmi.edu.

Shao-Qiu He, PhD, Department of Anesthesiology and Critical Care Medicine, Johns Hopkins University, School of Medicine, Baltimore, MD, 21205, USA. Phone: 410-502-0482; Fax: 410-502-0482; E-mail: shaoqiuh@hotmail.com.

Conflict-of-interest Statement

M.M., H.H. and S.C.T. are employed by BioTissue, Inc. However, none of the authors has a commercial interest in the material presented in this paper. There are no other relationships that might lead to a conflict of interest in the current study.

Abstract

Pain after surgery causes significant suffering. Opioid analgesics cause severe side effects and accidental death. Therefore, there is an urgent need to develop non-opioid therapies for managing post-surgical pain and, more importantly, preventing its transition to a chronic state. In a mouse model of post-surgical pain, local application of Clarix Flo (FLO), a human amniotic membrane (AM) product, attenuated established post-surgical pain hypersensitivity without exhibiting known side effects of opioid use in mice. Importantly, preemptive drug treatment also inhibited the transition of post-surgical pain to a prolonged state. This effect was achieved through direct inhibition of nociceptive dorsal root ganglion (DRG) neurons via CD44-dependent pathways, and indirect pain relief by attenuating immune cell recruitment. We further purified the major matrix component, the heavy chain-hyaluronic acid/pentraxin 3 (HC-HA/PTX3) from human AM that has greater purity and water solubility than FLO. HC-HA/PTX3 replicated FLO-induced neuronal and pain inhibition. Mechanistically, HC-HA/PTX3 induced cytoskeleton rearrangements to inhibit sodium current and high-voltage activated calcium current on nociceptive neurons, suggesting it is a key bioactive component mediating pain relief. Collectively, our findings highlight the potential of naturally derived biologics from human birth tissues as an effective non-opioid treatment for post-surgical pain and unravel the underlying mechanisms.

Keywords: pain; human birth tissues; sensory neurons; CD44; cytoskeleton rearrangement.

Introduction

Surgery or trauma may lead to persistent pain, impeding functional recovery and causing considerable distress.(1) Continuous reliance on opioid analgesics causes severe side effects and accidental death, which resulted in a national public health emergency being declared in 2017.(2) Accordingly, there is an urgent need to develop non-opioid alternative therapies for managing post-surgical pain and, more importantly, preventing its transition to a chronic state. An optimal strategy would be to develop local treatments that both inhibit pain and address the underlying pathophysiology, such as neuronal sensitization, inflammation, and delayed wound healing, while avoiding the central side effects of commonly used analgesics.(3)

A naturally occurring biologic derived from human birth tissues has recently gained our attention as a potential solution for this challenging problem. The birth tissue is predominantly comprised of the amniotic membrane (AM) and umbilical cord (UC), which share the same cell origin as the fetus. These versatile biological tissues have been used as medical therapy in a wide range of conditions.(4, 5) FLO (Clarix Flo; BioTissue, Miami, FL) is a sterile, micronized, and lyophilized form of human AM/UC matrix used for surgical and non-surgical repair, reconstruction, or replacement of soft tissue by filling in the connective tissue void. They have been shown to orchestrate regenerative healing within its anti-inflammatory and anti-scarring properties in ophthalmic applications.(6) Interestingly, FLO appears to relieve pain effectively in several ocular surface disorders,(7-9) and musculoskeletal disorders such as osteoarthritis(10, 11) and lower extremity neuropathy.(12) However, the mechanisms underlying their pain inhibition properties remain unknown.

In a plantar-incision mouse model of post-surgical pain, we explored whether FLO may be deployed as a viable biologic for the treatment and prevention of trauma pain, and examined the underlying mechanisms. We further purified the heavy chain-hyaluronic acid/pentraxin 3 (HC-HA/PTX3), which is in uniquely high amounts in human AM, and determined if HC-HA/PTX3 is a key bioactive component mediating pain relief. Our findings highlight the potential of a naturally derived biologic from human birth tissues as an effective non-opioid treatment for post-surgical pain and unravel the underlying mechanisms.

Results

1. FLO inhibited post-surgical pain and neuron activation.

Intra-paw injection of FLO, but not the vehicle (saline) acutely inhibited heat nociception in naïve wild-type (WT) mice (Fig 1A). Moreover, FLO dose-dependently (0.1-0.5 mg) attenuated heat hypersensitivity in the hindpaw receiving the plantar incision (Fig 1B), and inhibited mechanical hyperalgesia in the Randall-Sellito test (Fig 1C). In the Catwalk assay, FLO partially normalized the impaired gaiting caused by incision, as indicated by increases in print area and max contact area from pre-drug levels (Fig 1D, E), suggesting an attenuation of movement-evoked pain. FLO caused no impairment in locomotor function or exploratory activity in the open-field test (Fig 1F); these symptoms are known side effects of opioid use. The concentration of FLO we used fell within the range reported in previous clinical studies.(10, 13, 14)

Since nociceptive neuron hyperexcitability may lead to persistent pain,(15, 16) cellular mechanisms of pain inhibition by FLO can be partly inferred from its inhibition

of these neurons. We generated *Pirt-Cre*; *GCaMP6s* mice that exclusively express GCaMP6 (a fluorescent calcium indicator)(17) in primary sensory neurons to enable high-throughput *in vivo* calcium imaging of DRG neurons.(18, 19) (Fig 2A) Intra-paw injection of FLO selectively reduced the activation of small DRG neurons to noxious heat stimulation after plantar incision (Fig 2B-D).

2. Purified HC-HA/PTX3 mirrored *in vivo* pain inhibition by FLO.

We then purified Heavy chain 1-Hyaluronic acid/Pentraxin 3 (HC-HA/PTX3) from the water-soluble extract of human AM (Fig S1A, B), and biochemically and functionally characterized it using western blot and TRAP assays (Fig S1C-E).(20) The natural process of HC-HA/PTX3 formation may involve: Tumor necrosis factor-stimulated gene 6 protein covalently binds to HC1 of inter-alpha-trypsin inhibitor and then transfers it to high-molecular-weight hyaluronan (HMW-HA). At this point, HC1 becomes conjugated, and tumor necrosis factor-stimulated gene 6 is released. PTX3 then tightly associates with the HC1-HA complex by binding to the HC1.

HC-HA/PTX3 was suggested to be a biologically active component with uniquely high amounts in human birth tissues. (20-22) However, it was unclear whether the inhibitory effects of human AM products on pain and neuron activation were acted through it. Like FLO, intra-paw injection of HC-HA/PTX3 dose-dependently (10-20 μg) induced heat antinociception in naïve WT mice and attenuated heat hypersensitivity developed in the hindpaw after plantar-incision (Fig 3A). Moreover, HC-HA/PTX3-induced pain inhibition was comparable between male and female mice after plantar incision (Fig S2).

HMW-HA, a major component of HC-HA/PTX3, was suggested to attenuate inflammatory pain and the neuropathic pain induced by the cancer chemotherapy paclitaxel.(23-26) We wondered about the effect of HMW-HA on post-surgical pain. Importantly, we also compared the efficacy of HC-HA/PTX3 and HMW-HA, both at an amount of 20 μg since the weight of HC-HA/PTX3 was determined based on its HMW-HA content. At its peak (1 hour post-drug), HC-HA/PTX3 demonstrated a significantly more potent anti-hyperalgesic effect than HMW-HA. Importantly, this effect persisted for over 4 hours (Fig 3B). In contrast, the effect of HMW-HA had largely dissipated by approximately the 4-hour mark. Additionally, we tested the treatment using a mixture of HMW-HA and HC1, another important component of HC-HA/PTX3. Based on our previous findings, which demonstrated that 1 μg of HC-HA/PTX3 contained 1 μg of HMW-HA, 36 ng of HC1, and 10 ng of PTX3(27), we combined 20 μg of HMW-HA with 720 ng of HC1. However, this mixture did not demonstrate a greater pain-inhibitory effect compared to HMW-HA alone (Fig 3B).

3. HC-HA/PTX3 inhibited DRG neurons.

Mechanistically, HC-HA/PTX3 exerted DRG neuronal inhibitory effects in both *in vitro* calcium imaging (Fig 3C-F) and patch-clamp electrophysiology studies (Fig 3G, H). Transient receptor potential vanilloid 1 (TRPV1), transient receptor potential ankyrin 1 (TRPA1), and mas-related G protein-coupled receptor D (MrgprD)-expressing DRG neurons are critical to heat and mechanical pain signaling.(28) Applying capsaicin (a TRPV1 agonist), cinnamaldehyde (a TRPA1 agonist), or β-alanine (a MrgprD agonist) to bath solution increased intracellular calcium $[Ca^{2+}]_i$ in 41%, 24%, or 17% of DRG

neurons.(29, 30) Here, HC-HA/PTX3 (15 μg/mL) significantly reduced the $[Ca^{2+}]_i$ increase produced by these proalgesics. However, HMW-HA (15 μg/mL) was not effective (Fig 3C-F).

Intrinsic membrane excitability (IME) is a property of a neuron that refers to its general state of excitability, which is reflected in part by its ability to generate action potentials. While it is true that increased or decreased intrinsic excitability can imply how a neuron responds to a given input, it is reflective more of the neuron's output into the spinal cord. Further, IME is assessed in the neuron via current injected directly from the patch electrode, not from any exogenous stimulus. IME of DRG neurons from WT mice after plantar-incision was measured 24 h after dissociation. In small DRG neurons, HC-HA/PTX3 concentration-dependently hyperpolarized the membrane potential (5, 10, 25 μg/mL, Fig 3G, I), and increased the rheobase (Fig 3H, J), indicating decreased neuronal excitability. However, HC-HA/PTX3 (10 μg/mL) did not significantly affect the IME of large neurons (Fig S3A-H).

4. Pain inhibition by both FLO and HC-HA/PTX3 was CD44-dependent.

CD44 is a multifunctional transmembrane glycoprotein that functions as a cell surface adhesion receptor, regulating essential physiologic and pathologic processes.(31, 32) CD44 is the principal receptor for HA.(23) Since HMW-HA is a primary component of the HC-HA/PTX3 complex, we explored whether CD44 is also required for the inhibition of post-surgical pain by FLO and HC-HA/PTX3.

CD44 is expressed in both neurons and glial cells,(33) but its distribution in the DRG was unclear. In mouse DRG, CD44 immuno-reactivity highly colocalized with Na-

K ATPase alpha1, a neuron surface marker, but presented at a much lower level in satellite glial cells (Fig S4A). The specificity of the CD44 antibody was validated in CD44 knockout (KO) mice (Fig S4B) and by a previous study.(34) CD44 immuno-reactivity highly colocalized with CGRP and IB4, markers of small peptidergic and non-peptidergic nociceptive neurons (Fig 4A). Consistent with this finding, analysis of our recently published single-cell RNA-sequencing (scRNA-seq) dataset of mouse DRG showed high expression levels of CD44 in nociceptive neuronal clusters (Fig 4B),(35) but much lower expression in large neuronal clusters which are Aβ or Aδ low-threshold mechanoreceptors or proprioceptors, and in C-fiber low-threshold mechanoreceptors (c-LTMRs, Fig 4B). Another study also demonstrated the expression of CD44 in nociceptors but not in large DRG neurons.(36)

Importantly, in DRG neurons from CD44 KO mice, HC-HA/PTX3 did not reduce the capsaicin-evoked increase of $[Ca^{2+}]_i$ (Fig 4C-E), nor did it alter the IME and the membrane potential (Fig 4F, G). The basal IMEs were comparable between WT and CD44 KO mice (Table S1). Behaviorally, the inhibition of heat hyperalgesia by FLO (0.5 mg, 20 μL) and by HC-HA/PTX3 (10 or 20 μg, 20 μL) was both diminished in CD44 KO mice (Fig 4H, I). Likewise, applying a neutralizing antibody (IgG, 10 μg) to CD44, but not control IgG blocked HC-HA/PTX3-induced pain inhibition in WT mice (Fig 4J). Collectively, these findings suggest that pain inhibition, as well as the exclusive inhibition of small DRG neurons, which are mostly nociceptive, by HC-HA/PTX3 and FLO, are CD44-dependent.

5. HC-HA/PTX3 induced cytoskeletal rearrangement in DRG neurons.

We next explored how HC-HA/PTX3 induces CD44-dependent neuronal inhibition. CD44 signaling plays a vital role in regulating the cytoskeleton, forming an intricate fibrous subcellular network that undergoes dynamic changes to regulate cell function.(37) (38) Immunofluorescence staining showed that HC-HA/PTX3 (10, 15 μg/mL) significantly increased the translocation of F-actin to cell membranes in WT DRG neurons (Fig 5A, B). However, F-actin fibers were mostly retained in the cytoplasm in HMW-HA-treated (15 μg/mL) group. HC-HA/PTX3 at the concentration (0-15 μg/mL) tested did not induce neuronal toxicity, per the MTT assay (Fig 5C).

Increased sub-membranous F-actin after HC-HA/PTX3 treatment suggests greater availability of cortical actin filaments, accompanied by increased translocation of CD44 to the cell membrane (Fig 5A, B). These effects of HC-HA/PTX3 were prevented by a bath application of latrunculin-A (LAT-A, 1 μM, Fig 5A, B), an actin polymerization inhibitor that compromises the integrity of the cytoskeleton.(39) Moreover, knocking down of profilin-1 (*Pfn1*), an essential element for promoting actin polymerization,(40, 41) by electroporating DRG neurons with siRNA specifically targeting *Pfn1* (siPfn1) also diminished HC-HA/PTX3-induced cytoskeletal rearrangement (Fig 5D).

6. HC-HA/PTX3-induced cytoskeletal rearrangement depended on CD44 signaling.

Notably, pretreatment with CD44 IgG (2 μg/mL) blocked the cytoskeletal rearrangement induced by HC-HA/PTX3 (15 μg/mL, Fig 5E, F). In line with this finding, the condensation of sub-membranous F-actin and translocation of CD44 to the cell membrane after HC-HA/PTX3 were significantly increased only in small DRG neurons (Fig S5A, B), which express much higher levels of CD44 than large neurons (Fig 4A, B).

The downstream intracellular components involved in CD44-dependent cytoskeletal rearrangement induced by HC-HA/PTX3 remain unknown. CD44 may activate cytoskeletal proteins, such as *Ank2*-encoded Ankyrin-B and *Ank3*-encoded Ankyrin-G, which are highly expressed in DRG neurons and can modulate neuronal excitability.(42) CD44 can also interact with cortical actin filaments via ezrin/radixin/moesin (ERM) signaling.(43) Accordingly, we knocked down *Ank2* and *Ank3* together as siAnk group, and *Ezr*, *Rdx*, and *Msn* together as siERM group in cultured WT DRG neurons (Fig S6A, B). The mRNA levels of targeted genes were significantly decreased, but not abolished, after electroporation with the specific siRNAs (Fig S6C). Although HC-HA-PTX3 still increased the translocation of F-actin and CD44 to the cell membrane in both siAnk and siERM groups, the extent was significantly less than that in the siNT control group (Fig S6A, B), suggesting that both Ankyrin and ERM signaling may partly contribute to HC-HA/PTX3-induced cytoskeletal rearrangement.

7. Cytoskeletal rearrangement may contribute to the inhibition of ion channels by HC-HA/PTX3.

F-actin constitutes a sub-membranous cytoskeleton network, serving as an important scaffold for membrane ion channels, receptors, and intracellular kinases to function properly.(44) Analgesic mechanisms often involve modulation of ion channels, especially inhibiting high-voltage activated (HVA) calcium current (I_{ca}, e.g., morphine) and sodium current (I_{Nav}, e.g., lidocaine).(45-47)

Here, HC-HA/PTX3 (10 μg/mL) inhibited depolarization-elicited I_{Nav} in small DRG neurons from WT mice at day 2-4 after plantar-incision, compared to the vehicle (Fig

5G). In contrast, the same treatment increased I_{Nav} in CD44 KO mice (Fig S7A, B). Moreover, pretreatment with an intracellular infusion of LAT-A (0.5 nM) abolished the inhibition of I_{Nav} by HC-HA/PTX3 in WT mice; instead, an increased I_{Nav} was observed (Fig 5G, Fig S7B). LAT-A itself minimally affected I_{Nav}. HC-HA/PTX3 also inhibited the HVA-I_{ca} current in WT DRG neurons. This effect was also attenuated by intracellular infusion of LAT-A (Fig 5H, Fig S7C). These findings suggest that HC-HA/PTX3 may inhibit cell membrane ion channels through a CD44-mediated cytoskeleton rearrangement. Despite the cytoskeletal effects, neither bath application of HC-HA/PTX3 (15 μg/mL) nor intracellular infusion of LAT-A (0.5 nM) changed the gross morphology of DRG neurons (Fig S8).

8. Intra-operative FLO treatment inhibited the development of post-surgical pain.

Finally, we tested whether applying FLO to the wound right after plantar incision can exert a preemptive analgesic effect. Intra-operative FLO (1 mg) treatment significantly, but not entirely, attenuated heat hypersensitivity from day 1 to day 13 after the plantar incision (Fig 6A, B). FLO also reduced spontaneous pain, shown by decreased spontaneous foot lifting (SFL) count and duration at day 3 post-injury (Fig 6C). Moreover, the impaired animal's gaiting was alleviated by preemptive FLO treatment in the Catwalk assay (Fig 6D, E), suggesting relief of movement-evoked pain. Inflammation sensitizes neurons and contributes to pain chronicization.(1) Our previous work(48) and flow cytometry study showed that plantar incision induced profound immune cell recruitment and mast cell aggregation near the wound (Fig 6F, G). An intra-operative FLO (1 mg) treatment markedly reduced leukocyte ($CD45^+$ cells),

$CD11b^{+}Ly6G^{+}$ neutrophil and $CD11b^{+}Ly6G^{-}Ly6C^{+}$ monocyte recruitments (Fig 6F, Fig S9). Mast cells are central to recruiting inflammatory cells. Indeed, the FLO-treated group also showed significantly decreased *Mrgprb2-Cre tdT*$^{+}$ mast cell aggregation near the wound site (Fig 6G). Thus, FLO may reduce immune cell recruitment, possibly limiting inflammation which represents an indirect mode of anti-pain action.

Conclusions

Our study suggests that human birth tissue products may be deployed as a viable biologic to treat post-surgical pain. Mechanistically, FLO may work by reducing the excitability of nociceptive DRG neurons and decreasing immune cell recruitment. We also identified HC-HA/PTX3 as the primary bioactive component responsible for pain inhibition. It induced an acute cytoskeleton rearrangement and inhibition of I_{Nav} and HVA-I_{ca} currents in a CD44-dependent manner. The multiple modes of action of human birth tissue products suggest they may not only alleviate pain symptoms but also address the underlying causes, making them a promising non-opioid treatment for post-surgical pain and its prevention.

Discussion

Our study revealed that human birth tissue products (FLO) mitigated post-surgical pain by directly inhibiting nociceptive neurons, and indirectly via reducing immune cell recruitment. The major matrix component purified from human AM, HC-HA/PTX3, mimics the pain and neuronal-inhibitory effects of FLO. Mechanistically, both compounds exert pain inhibition in a CD44-dependent manner. At the cellular level, HC-

HA/PTX3 caused membrane hyperpolarization, modified the intrinsic properties, and inhibited I_{Nav} and HVA-I_{ca} in nociceptive DRG neurons through cytoskeleton rearrangement and interaction with these membrane ion channels.

Applying FLO locally inhibited heat and mechanical hyperalgesia, spontaneous pain, and movement-induced pain in WT mice following plantar incision. Similarly, HC-HA/PTX3 also inhibited heat hyperalgesia. Intriguingly, treatment with HC-HA/PTX3 demonstrated a stronger and longer-lasting pain-inhibitory effect compared to treatment with HMW-HA and the combination of HMW-HA and HC1, at their comparable dosages tested. This finding suggests the superiority of HC-HA/PTX3 over HMW-HA for post-surgical pain treatment, yet the underlying mechanisms remain unknown. After *in vivo* administration, HMW-HA undergoes rapid and progressive degradation through a series of enzymatic reactions, resulting in the formation of polymers of decreasing sizes and altered bioactivity. Notably, different sizes of HA fragments exhibit a wide range of biological functions, which are sometimes opposing. For example, larger hyaluronan polymers (e.g., HMW-HA) possess anti-angiogenic, immunosuppressive, and anti-hyperalgesic properties. In contrast, smaller polysaccharide fragments are often inflammatory, immuno-stimulatory, angiogenic, and proalgesic. Moreover, they can compete with larger hyaluronan polymers for target receptors.(49) The long-lasting drug action of HC-HA/PTX3 *in vivo* indicates that it may possess a more stable structure than HMW-HA, making it less prone to degradation.

Small DRG neurons are activated by heat and noxious stimulation, while innocuous mechanical stimulation mainly activates large DRG neurons and low-threshold mechanoreceptors (LTMRs)(50). Both FLO and HC-HA/PTX3 inhibited small DRG

neurons, as evidenced by decreased excitability in functional GCaMP6s imaging and electrophysiologic recording. We found that the potent neuronal inhibitory effect of HC-HA/PTX3 may result from their high expression of CD44. Both pain and neuronal inhibitory effects from FLO and HC-HA/PTX3 were CD44-dependent. Importantly, scRNA-seq analysis showed a significantly higher expression of CD44 in small nociceptive DRG neurons, compared to large neurons (e.g., LTMRs and proprioceptors). Similar findings were also observed in DRG scRNA-seq datasets from another two studies.(36, 51) In line with this notion, HC-HA/PTX3 exerted a minimal effect on large DRG neurons. Nevertheless, the mechanisms for the differential drug effects warrant further investigations.

Unlike traditional analgesics, which often target a single downstream effector, HC-HA/PTX3 may induce a range of changes that could fundamentally decrease nociceptor excitability. These changes include membrane hyperpolarization, altered intrinsic membrane properties, and the inhibitions of multiple membrane ion channels, including I_{Nav} and HVA I_{ca}. In addition, HC-HA/PTX3 reduced calcium responses evoked by several proalgesic compounds, including capsaicin, β-Alanine, and cinnamal in nociceptive DRG neurons. The activations of TRPV1, MrgprD, and TPRA1 are known to be important to heat and mechanical hypersensitivity and themselves are important targets for pain control. Therefore, HC-HA/PTX3 can effectively block the transmission of noxious afferent inputs through multiple modes of action.

To explore the molecular basis of HC-HA/PTX3-induced neuronal inhibition, our study unraveled that HC-HA/PTX3, but not HMW-HA, induced a rearrangement of the cytoskeleton, leading to an increase in sub-membranous F-actin polymerization and the

translocation of CD44 to the vicinity of the cell membrane in small DRG neurons. This effect was not observed in large neurons, and was blocked by both LAT-A pretreatment and Pfn1 knockdown, which disrupt actin polymerization. Given that polymerized F-actin serves as a scaffold for signaling that affects ion channels, we speculate that the cytoskeleton rearrangement triggered by HC-HA/PTX3 could thus profoundly change ion channel function and, consequently, neuronal excitability. Supporting this hypothesis, the intracellular infusion of a low dose of LAT-A, which had minimal effect on I_{Nav}, and HVA-I_{ca} and the morphology of DRG neurons, blocked the inhibition of I_{Nav} and HVA-I_{ca} by HC-HA/PTX3. Thus, HC-HA/PTX3 may inhibit ion channels through a CD44-mediated cytoskeleton rearrangement, representing a novel mechanism for neuron inhibition.

The signaling of HMW-HA also depends on CD44 clustering in lipid rafts, and disrupting this markedly reduces HMW-HA-induced anti-hyperalgesia.(24) However, at the concentration tested (15 μg/mL), HMW-HA did not increase cortical F-actin and CD44 translocation in small DRG neurons, nor attenuated capsaicin-induced $[Ca^{2+}]_i$ increase. These findings suggest that different ligands may induce varying cellular effects after binding to CD44. Indeed, HA of different molecular weights can activate different downstream signaling pathways of CD44, leading to opposing effects. For example, HMW-HA produced anti-hyperalgesia, while low-molecular-weight HA (LMW-HA) induced hyperalgesia.(23) While Src signaling was involved in LMW-HA-induced hyperalgeisa,(24) other downstream signaling pathways of CD44s participated the anti-hyperalgesic effect of HMW-HA, including phosphatidylinositol (PI) 3-kinase gamma (PI3Kγ)/ protein kinase B (AKT), RhoGTPases (RhoA and Rac1), phospholipases

(phospholipases Cε and Cγ1).(24-26) These findings suggest a complex interplay of downstream signaling pathways of CD44 in pain modulation.

HMW-HA was reported to attenuate CIPN only in male rats.(25) However, sex dimorphism was not observed in the inhibition of PGE2-induced inflammatory pain by HMW-HA.(24) Similarly, HC-HA/PTX3 induced comparable pain inhibition in both sexes. For LMW-HA-induced hyperalgesia, three receptors, including CD44, toll-like receptor 4 (TLR4), and receptor for hyaluronan-mediated motility (RHAMM), may be involved. Yet, estrogen dependence was only established for RHAMM-dependent hyperalgesia and its inhibition by HMW-HA.(52) These findings collectively suggest a complex interplay between estrogen and different types of HA and HA receptors in pain regulation.

The proactive prevention of post-surgical pain would be highly beneficial and describable. Although peri-surgery nerve blocks have been used to mitigate post-surgical pain, the effect is short-lasting. To our knowledge, preemptive treatment to induce a prolonged inhibition of post-surgical pain remains unavailable. Here, an intra-operative FLO treatment prevented post-surgical pain, which may be partly attributable to its anti-inflammatory drug action. Non-resolving inflammation can impair healing and hinder the effectiveness of pain therapies. HC-HA/PTX3 may exert anti-inflammatory actions and help maintain stem cell quiescence,(21, 53) thereby supporting tissue homeostasis and repair. Activation of Mrgprb2-Cre tdT^{+} mast cells can release multiple inflammatory mediators beyond tryptase and TNFα, and stabilization of mast cells could attenuate post-surgical pain.(48) FLO reduced aggregation of mast cells and other immune cells at the wound site, which might limit crosstalk between these cells and neurons implicated in

post-surgical pain.(54) We have previously shown that HC-HA/PTX3 also promotes the polarization of murine macrophage into the anti-inflammatory M2 phenotype.(22) Therefore, FLO may help limit local inflammatory response and facilitate pain resolution after surgery.

Materials and Methods

1 Animals

C57BL/6 mice and CD44 KO mice (B6.129(Cg)-Cd44tm1Hbg/J, strain #005085)(34) were purchased from Jackson (Jax) Laboratories. The *Pirt-Cre* mice, *Rosa26-lox-stop-lox GCaMP6s* mice, and *Mrgprb2-Cre tdT* mice were generated by Dr. Xinzhong Dong in the Solomon H Snyder Department of Neuroscience, School of Medicine, Johns Hopkins University.

Sex as a biological variable

Our study examined male and female animals, and similar findings are reported for both sexes.

2 Paw plantar incision model of post-surgical pain

Paw plantar-incision was performed as described in previous studies.(55) A 5-mm longitudinal incision was made through the skin and fascia of the plantar aspect, beginning 2 mm from the proximal edge of the heel and extending toward the toes. The flexor muscle was elevated with curved forceps.

3 Animal behavioral tests

3.1 Hargreaves test for heat hyperalgesia

The paw withdrawal latency was tested as described in our previous study (56) with 30 seconds as the cutoff time. Each hind paw was stimulated 3 times at an interval > 5 minutes.

3.2 Randall-Selitto test for mechanical hyperalgesia

The test consisted of applying the increasing mechanical force using the tip of Randall Selitto (IITC 2500) apparatus to the dorsal surface of the mouse hind paw. A total of three repeated tests were performed for each paw. Animal responses, including discomfort/struggle, paw withdrawal, and vocal responses, were observed as an endpoint of the result. The force resulting in any of the end-point behaviors was considered as the mechanical threshold. The cutoff force was 250 g.

3.3 CatWalk gait analysis

CatWalk XT version 10.6 gait analysis system (Noldus Information Technology, Wageningen, Netherlands) was used.(56) At least three compliant runs were collected at each time point. The following parameters were investigated: a) Print area, b) Max contact area, c) Max contact intensity. To rule out the confounding influences of body weight and paw size, the walking parameters of the LH (injured side) were normalized by that of RH (uninjured side).

3.4 Open field test

Locomotor activity was monitored and quantified using a Photobeam Activity System-

Open Field (PAS-OF) (San Diego Instruments, San Diego, CA). The total number of beam breaks over the second 30 min was analyzed. On post-injury day 2, the first round of open field test was conducted without drug treatment. On post-injury day 4, mice received an intra-paw injection of the vehicle or FLO 30 min prior to the test.

3.5 Spontaneous pain behavior measurement

Spontaneous pain behavior was examined as previously described.(57) The video recording lasted for 30 minutes.

4 *In vivo* calcium imaging in mice

The L4 DRG of *Pirt-Cre*; *GCaMP6s* mice were exposed for imaging as described in our previous studies.(18, 58) Mice under anesthesia (1.5% isoflurane) were laid on a custom-designed microscope stage with the spinal column being stabilized. Live images of the intact DRG were acquired at five frames with 600 Hz in frame-scan mode, using a 10X/0.30 long-working distance air objective lens (Leica, 506505) of a confocal microscope (Leica TCS SP8, Wetzlar, Germany). Dipping the hind paw into a 51°C water bath was applied as noxious heat stimulation.

Raw image stacks were imported into FIJI (NIH) for imaging data analysis. To measure the maximum fluorescence intensity (F_t), the average pixel values in a given region of interest (ROI) were calculated for each image frame recorded during the whole recording period. A ratio of fluorescence difference ($\Delta F = F_t - F_0$) to baseline level (F_0) ≥ 30% was defined as an activation of the neuron. Somal areas of < 450 μm2, 450 to 700 μm2, and >700 μm2 were used for defining small, medium, and large DRG neurons,

respectively.

5 Immunocytochemistry

Mice were deeply anesthetized and perfused with 30 mL 0.1 M PBS (pH 7.4, 4°C) followed by 30 mL paraformaldehyde (PFA) solution 4% (vol/vol) in PBS (4°C).(48) DRG and skin were dissected and post-fixed in 4% PFA at 4°C for 2 hours, then sectioned (15 µm width) with a cryostat. The slides were pre-incubated in a blocking solution and stained with indicated primary antibodies and corresponding secondary antibodies.

The slides were pre-incubated in blocking solution and stained against Griffonia simplicifolia isolectin GS-IB4 Alexa 568 (Invitrogen, I21412; 1:500), Neurofilament 200 (Sigma-Aldrich, N5389; 1:500), CGRP (Cell Signaling Technology, 14959; 1:200), Na+/K+ ATPase α-1 (Sigma-Aldrich, 05-369; 1:200), GFAP (Millipore, MAB360; 1:500), CD44 (Cell Signaling Technology, 3570; 1:500) and corresponding Alexa Fluor-conjugated secondary antibodies (1:500, Thermo Fisher Scientific). Raw confocal (TIFF) images (LSM 700; Zeiss, White Plains, NY, USA) were analyzed with Fiji (NIH). The total number of neurons in each section was determined by counting both labeled and unlabeled cell bodies. Positively stained neurons had clear stomata and an increase in fluorescence intensity ≥30% of the background. To quantify the neuronal cross-sectional area of DRG neurons, cells were identified by morphology with a clearly defined, dark, condensed nucleus. Positively stained cells were chosen for cross-sectional area measurement. The soma of the labeled cells was traced manually with the Fiji 'Freehand selection' tool, and the areas were measured. Tissues from different groups were

processed together.

6 Immunoblotting

The tissues were lysed in radioimmunoprecipitation assay (RIPA) buffer (Sigma, St. Louis, MO) containing a protease/phosphatase inhibitor cocktail (Cell Signaling Technology, Boston, MA). Samples (20 μg) were separated on a 4% to 12% Bis-Tris Plus gel (Thermo Fisher Scientific) and then transferred onto a polyvinylidene difluoride membrane (Thermo Fisher Scientific). Immunoreactivity was detected by enhanced chemiluminescence (ECL; Bio-Rad, Hercules, CA) after incubating the membranes with the indicated primary antibody (4°C, overnight).

Antibodies were chosen based on previous findings and our own study. GAPDH (EMD Millipore, 1: 100,000) was used as an internal control for protein loading. CD44 (EMD Millipore, MABF580; 1:2000) was validated by a previous study.(34) ImageJ (ImageJ 1.46r) was used to quantify the intensity of immunoreactive bands of interest on autoradiograms.

7 *In vitro* calcium imaging

Experiments were conducted as described in our previous studies.(35) Neurons were loaded with the fluorescent calcium indicator Fura-2-acetomethoxyl ester (2 μg/mL, Molecular Probes, Eugene, OR) for 45 mins in the dark at room temperature and then allowed to de-esterify for 15 min at 37 °C in the warm external solution. Cells were imaged at 340 and 380 nm excitation for the detection of intracellular free calcium.

8 Immune cell recruitment assays

8.1 Flow cytometry study

FLO (1 mg) or the vehicle was applied to the wound right after the plantar incision and kept throughout the surgery and after suturing. Hind paw skin was collected 24 hours after surgery using a 6-mm biopsy punch and placed in dissociation media (37°C, 75 min). Among the live cells, neutrophils were gated as $CD11b^{+}Ly6G^{+}$, monocytes were gated as $CD11b^{+}Ly6G^{-}Ly6C^{+}$. Data was collected with a CytoFLEX LX (Beckman Coulter) and analyzed by FlowJo (TreeStar). The staining included the use of antibodies against mouse CD45 (Biolegend, 103108); mouse Ly6C (Biolegend, 128016); mouse Ly6G (Biolegend, 127628); mouse/human CD11b (Biolegend, 101243).

8.2 Mast cell quantification

Mrgprb2-Cre tdT mice (tdTomato fluorescent protein under the Mrgprb2 promoter) were used to label mast cells.(48) To quantify the number of mast cells per mm^2, at least 10 fields randomly captured from > 6 non-adjacent sections in each mouse were analyzed. For each mouse, the mast cell count per mm^2 was calculated by dividing the total number of mast cells by the total area analyzed.

9 Cell viability assay (MTT assay)

Cell viability was evaluated by the MTT assay (Roche, 11465007001). DRG cells were seeded in 96-Well microplates and subsequently exposed to several concentrations of HC-HA/PTX3 (0.5 µg – 15 µg/mL) with an incubation time of 24 hours at 37°C. After the treatments, the medium was removed and 10 µL of the MTT labeling reagent (final

concentration 0.5 mg/mL) was added to each well. Optical density was measured in a spectrophotometer (Molecular Devices, FlexStation 3 Multi-Mode Microplate Reader) at 490 and 650 nm. Cell survival was expressed as the percentage of formazan absorbance, compared to the pretreatment level (experimental/control).

10 Immunofluorescence of CD44 and F-actin in DRG neurons

Cultured lumbar DRGs were plated on an 8 mm glass coverslip. DRG neurons were then exposed to HC-HA/PTX3 [10 or 15 μg/mL with or without latrunculin-A (LAT-A, 1 μM, Invitrogen, L12370)] for 45 min at 37 °C. Cells were fixed for 10 minutes in 4% paraformaldehyde. The cover slips were then permeabilized with 0.3% Triton X-100 and sequentially stained with rat anti-CD44 antibody (BD Biosciences, 550538; 1:200), and corresponding Alexa 488-conjugated secondary antibodies (Invitrogen, A-11006; 1:500). The F-actin were stained with Alexa 568-conjugated phalloidin (Invitrogen, A12380; 1:400).

Raw confocal images (TIFF) were analyzed with Fiji (NIH). To quantify the changes in fluorescence of phalloidin and CD44 after drug treatment, the positive staining distributed along the whole plasma membrane and localized within the cell cytoplasm were traced manually with the Fiji “Freehand selection” tool and the fluorescence intensity were measured. The proportion of staining on the plasma membrane was determined as a percent of the total staining measured in a cell.

11 Electrophysiology

11.1 Whole-cell patch-clamp recording of DRG neurons

Patch-clamp electrodes were conducted as described in our previous studies,(59) Briefly, for current-clamp recordings of intrinsic excitability, neurons were perfused with an oxygenated solution composed of (in mM) 140 NaCl, 4 KCl, 2 $MgCl_2$, 2 $CaCl_2$, 10 HEPES, and 10 glucose (pH = 7.4; ~305–310 mOsm). The internal solution was composed of (in mM) 135 K-Gluconate, 10 KCl, 10 HEPES, 2 Na_2ATP, 0.4 Na_2GTP, and 1 $MgCl_2$ (pH = 7.4 with KOH; ~300–305 mOsm).

For I_{Nav} recordings, neurons were perfused with an oxygenated solution consisting of (in mM): 80 $NaCl_2$, 50 Choline-Cl, 30 TEA-Cl, 2 $CaCl_2$, 0.2 $CdCl_2$, 10 HEPES, 5 glucose (pH = 7.3; ~310-320 mOsm). The internal solution was composed of (in mM): 70 $CsCl_2$, 30 $NaCl_2$, 30 TEA-Cl, 10 EGTA, 1 $CaCl_2$, 2 $MgCl_2$, 2 Na_2ATP, 0.05 Na-GTP, 10 HEPES, 5 glucose (pH = 7.3 adjusted with CsOH; ~310 mOsm). For HVA-I_{Ca} recordings, neurons were perfused with an oxygenated solution consisting of (in mM) 130 N-methyl-D-glucamine chloride (NMDG-Cl; solution of 130 mM NMDG pH =7.4), 5 $BaCl_2$, 1 $MgCl_2$, 10 HEPES, and 10 glucose (pH = 7.4; ~310–315 mOsm adjusted with sucrose). The internal solution was composed of (in mM) 140 TEA-Cl, 10 EGTA, 1 $MgCl_2$, 10 HEPES, 0.5 Na_2GTP, and 3 Na_2ATP (pH = 7.4; ~300–305 mOsm). In some experiments, 0.5 nM LAT-A or vehicle was added to the internal solution and infused into the neuron via the patch pipette.

All recordings were filtered at 4 kHz, sampled at a rate of 20 kHz, and stored on a personal computer (Dell) using pClamp 11 and a digitizer (Digidata 1550B, Molecular Devices). Currents were digitally filtered offline by using a low-pass Gaussian filter with a -3 dB cut-off set to 2 kHz (Clampfit software; pClamp 11, Molecular Devices).

11.2 Intrinsic excitability studies of DRG neurons

After obtaining whole-cell configuration in both small-diameter DRG neurons (≤ 20 µm diameter) and large DRG neurons (≥ 50 µm diameter) from mice after bilateral plantar incision, a 5-min equilibration period was allowed. First, the spontaneous activity of the neuron was recorded for 1-2 min from V_{rest}. Additional intrinsic excitability measurements were then made before and after the bath application of 10 µg/ml HC-HA/PTX3. Rheobase was measured by injecting a series of square-wave current steps via the patch electrode (500 ms, 10 pA steps) until a single action potential (AP) was generated. Additionally, pre-drug AP threshold (mV), AP amplitude (mV), AP half-width (msec), and input resistance (MΩ) were measured before and after drug application. All measurements were compared using paired t-tests.

11.3 I_{Nav} studies of DRG neurons

Under voltage-clamp conditions, whole-cell I_{Nav} currents were normalized to each cell capacitance measurement to examine current density (pA/pF). For examination of I_{Nav} current-voltage (I-V) relationships and steady-state activation, after 5-min infusion of 0.5 nM LAT-A or vehicle, a series of 50 msec depolarizing square wave voltage steps were delivered via the patch electrode (V_{hold} = -90 mV; Vt_{est} = -80 mV to +60 mV, 10 mV steps). 10 µg/ml HHP was then applied via bath perfusion for 4 mins before the I_{Nav} I-V protocol was run again. The current-voltage relationship (I-V curve) was ascertained by plotting normalized peak I_{Nav} amplitudes at each test voltage (-80 mV to +60 mV). The voltage dependency of I_{Nav} steady state activation was determined by plotting normalized peak Na conductances (G_{Na}/G_{max}) at each test voltage. G_{Na} was computed by: $G_{Na} = I_{Nav}$ /

($V-V_{rev}$), where I_{Nav} is the maximum sodium current during test voltage application. Data were then normalized to the maximum Na conductance (G_{max}), then fitted to a Boltzmann distribution:

$$G_{Na}/G_{Max} = \frac{1}{1 + \exp\left[ze\frac{(V - V_{half})}{kT}\right]}$$

Where V_{half} is the potential for half max activation, k is the Boltzmann constant, z is an apparent gating charge, T is the absolute temp, and KT/e = 25 mV at 22º C. I_{Nav} I-V relationships and normalized conductances were compared using two-way RM ANOVA.

11.4 HVA-I_{Ca} studies of DRG neurons

In small-diameter DRG neurons (≤ 20 µm), whole-cell HVA-I_{Ca} currents were normalized to each cell capacitance measurement to examine current density (pA/pF). For examination of HVA-I_{Ca} current-voltage (I-V) relationships and channel open probabilities, after a 5-min infusion of 0.5 nM LAT-A or vehicle, a series of 25 msec depolarizing square wave voltage steps were delivered via the patch electrode (V_{hold} = -80 mV; V_{test} = -70 mV to +40 mV, 10 mV step). 10 µg/ml HC-HA/PTX3 was then applied via bath perfusion for 4 mins before the HVA-I_{Ca} I-V protocol was run again. The current-voltage relationships (I-V curves) were ascertained by plotting normalized peak HVA-I_{Ca} amplitudes at each test voltage (-70 mV to +40 mV). The voltage dependency of HVA-I_{Ca} channel open probability was determined by plotting normalized tail currents as a function of test voltages applied, which were then fitted with a Boltzmann equation for

channel open probabilities:

$$P(V) = P_{min} + \frac{P_{max} - P_{min}}{1 + e^{\frac{V - V_{half}}{k}}}$$

P(V) represents the channel open probability as a function of membrane potential; Pmin and Pmax are the minimum and maximum open probabilities; V_{half} is the voltage at 50% maximum current; and k is the default slope value.

12 Nucleofection

The dissociated neurons from lumbar DRGs were suspended in 100 µL of Amaxa electroporation buffer (Lonza Cologne GmbH, Cologne, Germany) with siRNAs (0.2 nmol per transfection). Suspended cells were transferred to a 2.0 mm cuvette and electroporated with the Amaxa Nucleofector apparatus. After electroporation, cells were immediately mixed to the desired volume of prewarmed culture medium and plated on precoated coverslips or culture dishes.

13 Quantitative PCR

Total RNA was isolated using PicoPure RNA Isolation Kit (Thermo Fisher Scientific) following the manufacturer's manual. RNA quality was verified using the Agilent Fragment Analyzer (Agilent Technologies, Santa Clara, CA). Two-hundred ng of total RNA was used to generate the cDNA using the SuperScript VILO MasterMix (Invitrogen, Waltham, MA). 10 ng of cDNA was run in a 20 µl reaction volume

(triplicate) using PowerUp SYBR Green Master Mix to measure real-time SYBR green fluorescence with QuantStudio 3 Real-Time PCR Systems (Thermo Fisher Scientific). Calibrations and normalizations were performed using the $2^{-\Delta\Delta CT}$ method.

Mouse *Gapdh* was used as the reference gene.

14 FLO

FLO (Clarix Flo; BioTissue, Miami, FL) is a sterile, micronized and lyophilized form of human amniotic membrane (AM) and umbilical cord (UC) matrix used for surgical and non-surgical repair, reconstruction or replacement of soft tissue by filling in the connective tissue void. Clarix Flo is regulated under section 361 of the Public Health Service Act and the regulations in 21 CFR Part 1271. Clarix Flo is derived from donated human placentas delivered from healthy mothers and is then aseptically processed to devitalize all living cells but retain the natural characteristics of the tissue.

15 Qualification and release of HC-HA/PTX3

HC-HA/PTX3 was purified from human amniotic membrane (AM) after donor eligibility was determined according to the requirements by FDA based on our published method(20) with modifications and was performed according to good laboratory practices (GLP). All standard operating procedures (SOPs), work instructions, and forms used for release testing were approved by the quality assurance department of Biotissue, inc. and the testing was performed according to GLP. The purity of HC-HA/PTX3 was disclosed by the lack of detectable proteins per BCA assay with a detectable level of 11.7±3.2 μg/ml and notable reduction of protein bands per silver staining in AM4P when compared

to AM2P with or without NaOH, which cleaves the ester bond between HA and HC1 (Fig. S1A). Due to the lack of detectable proteins, HC-HA/PTX3 was tested based on the amount of HA. HA in HC-HA/PTX3 was of high molecular weight (HMW) (≥ 500 kDa) when compared to the HMW HA control using agarose gel electrophoresis (Fig. S1B). It was released by confirming the identity of HC-HA/PTX3 based on Western blot analysis using respective antibody specific to HC1 (ITIH1 antibody, Cat# ab70048, Abcam, Waltham, MA, USA) and PTX3 (PTX3 antibody, Cat# ALX-804-464-C100, Enzo, Farmingdale, NY, USA) with or without hyaluronidase (HAase) digestion to release HC1 and HMW PTX3 from HC-HA/PTX3 in the loading well into the gel and with or without reduction by DTT, which further rendered PTX3 from HMW (octamer) to dimer and monomer (Fig. S1C, D). In addition, each batch of HC-HA/PTX3 was released after it also passed the potency assay (Fig. S1E), with the acceptance criterion of no less than (NLT) 89.21% inhibition of tartrate-resistant acid phosphatase (TRAP) activity of osteoclast differentiation in cloned monocytes of murine RAW264.7 cell line (ATCC, Manassas, VA, USA) by receptor activator of nuclear factor kappa-B ligand (RANKL) (PeproTech, Cranbury, NJ, USA).

16 Statistical analysis

Statistical analyses were performed with the Prism 9.0 statistical program (GraphPad Software, Inc). The methods for statistical comparisons in each study were indicated in the figure legends. To reduce selection and observation bias, animals were randomized to the different groups and the experimenters were blinded to drug treatment. The comparisons of data consisting of two groups were made by Student's t-test.

Comparisons of data in three or more groups were made by one-way analysis of variance (ANOVA) followed by the Bonferroni post hoc test. Comparisons of two or more factors across multiple groups were made by two-way ANOVA followed by the Bonferroni post hoc test. Two-tailed tests were performed, and $p<0.05$ was considered statistically significant in all tests.

Study approval

The Johns Hopkins University Animal Care and Use Committee (Baltimore, MD, USA) approved animal studies that were consistent with the National Institutes of Health Guide for the Care and Use of Laboratory Animals to ensure minimal animal use and discomfort.

Author Contributions

S.-Q.H., S.C.T. and Y.G. conceived the study and designed the project; C.Z., Q.H., N.C.F., S.-Q.H., N.L., Q.L., F.Y., X.C., A.U., J.L., M.M., H.H., X.-W.W, I.D., Y.-R.W, J.-R.W, and G.-W.Z conducted the experiments; C.Z., Q.H., N.C.F., and S.-Q.H. analyzed data; C.Z. and Y.G. wrote the manuscript with contributions from all authors. S.N.R., H.-P.J., D.-Z.Y., X.-Z.D. and S.C.T. were involved in some experimental design, discussion of results, and manuscript review.

Acknowledgments

The authors thank Kristy Hamlin, Monica Cuellar Entrena, and Melissa Suarez from BioTissue, Inc. for their work preparing and characterizing HC-HA/PTX3. The authors

also thank Drs. Courtney McQueen and Anne N. Connor (Senior Science Writers, Research Development Team, Office of the Vice Provost for Research, Johns Hopkins University) for editing the manuscript.

Funding

This study was supported by the National Institutes of Health (NIH, Bethesda, Maryland, USA) grants NS110598 (Y.G.), NS117761 (Y.G.), by the Lerner Family Fund for Pain Research (N.C.F). X.-W.W. was supported by an NIH grant K99EY031742. Funders had no role in study design, data collection, data interpretation, or the decision to submit the work for publication. Y.G. and S.N.R. received research grant support from Medtronic, Inc.

References

1. Kehlet H, Jensen TS, and Woolf CJ. Persistent postsurgical pain: risk factors and prevention. *Lancet.* 2006;367(9522):1618-25.
2. Colvin LA, Bull F, and Hales TG. Perioperative opioid analgesia-when is enough too much? A review of opioid-induced tolerance and hyperalgesia. *Lancet.* 2019;393(10180):1558-68.
3. Patapoutian A, Tate S, and Woolf CJ. Transient receptor potential channels: targeting pain at the source. *Nat Rev Drug Discov.* 2009;8(1):55-68.
4. de Rotth A. Plastic repair of conjunctival defects with fetal membranes. *Arch Ophthalmol-Chic.* 1940;23(3):522-5.
5. Chao YC, Humphreys S, and Penfield W. A New Method of preventing Adhesions. The Use of Amnioplastin after Craniotomy. *Br Med J.* 1940;1(4134):517-38 1.
6. Tighe S, Mead OG, Lee A, and Tseng SCG. Basic science review of birth tissue uses in ophthalmology. *Taiwan J Ophthalmol.* 2020;10(1):3-12.
7. Espana EM, Grueterich M, Sandoval H, Solomon A, Alfonso E, Karp CL, et al. Amniotic membrane transplantation for bullous keratopathy in eyes with poor visual potential. *J Cataract Refract Surg.* 2003;29(2):279-84.
8. Morkin MI, and Hamrah P. Efficacy of self-retained cryopreserved amniotic membrane for treatment of neuropathic corneal pain. *Ocul Surf.* 2018;16(1):132-8.
9. Finger PT. Finger's amniotic membrane buffer technique: protecting the cornea during radiation plaque therapy. *Arch Ophthalmol.* 2008;126(4):531-4.
10. Castellanos R, and Tighe S. Injectable Amniotic Membrane/Umbilical Cord Particulate for Knee Osteoarthritis: A Prospective, Single-Center Pilot Study. *Pain medicine (Malden, Mass).* 2019;20(11):2283-91.
11. Mead OG, and Mead LP. Intra-Articular Injection of Amniotic Membrane and Umbilical Cord Particulate for the Management of Moderate to Severe Knee Osteoarthritis. *Orthop Res Rev.* 2020;12:161-70.
12. Buksh AB. Ultrasound-guided injections of amniotic membrane/umbilical cord particulate for painful neuropathy of the lower extremity. *Cogent Medicine.* 2020;7(1):1724067.
13. Ackley JF, Kolosky M, Gurin D, Hampton R, Masin R, and Krahe D. Cryopreserved amniotic membrane and umbilical cord particulate matrix for partial rotator cuff tears: A case series. *Medicine (Baltimore).* 2019;98(30):e16569.
14. Bennett DS. Cryopreserved amniotic membrane and umbilical cord particulate for managing pain caused by facet joint syndrome: A case series. *Medicine.* 2019;98(10):e14745.
15. Xie W, Strong JA, Meij JTA, Zhang JM, and Yu L. Neuropathic pain: early spontaneous afferent activity is the trigger. *Pain.* 2005;116(3):243-56.
16. Zimmermann M. Pathobiology of neuropathic pain. *Eur J Pharmacol.* 2001;429(1-3):23-37.
17. Chen TW, Wardill TJ, Sun Y, Pulver SR, Renninger SL, Baohan A, et al. Ultrasensitive fluorescent proteins for imaging neuronal activity. *Nature.* 2013;499(7458):295-300.
18. Zheng Q, Xie W, Luckemeyer DD, Lay M, Wang XW, Dong X, et al. Synchronized cluster firing, a distinct form of sensory neuron activation, drives spontaneous pain. *Neuron.* 2022;110(2):209-20 e6.
19. Kim AY, Tang Z, Liu Q, Patel KN, Maag D, Geng Y, and Dong X. Pirt, a phosphoinositide-binding protein, functions as a regulatory subunit of TRPV1. *Cell.* 2008;133(3):475-85.
20. He H, Li W, Tseng DY, Zhang S, Chen SY, Day AJ, and Tseng SC. Biochemical characterization and function of complexes formed by hyaluronan and the heavy chains of inter-alpha-inhibitor (HC*HA) purified from extracts of human amniotic membrane. *J Biol Chem.* 2009;284(30):20136-46.
21. Chen SY, Han B, Zhu YT, Mahabole M, Huang J, Beebe DC, and Tseng SC. HC-HA/PTX3 Purified From Amniotic Membrane Promotes BMP Signaling in Limbal Niche Cells to Maintain Quiescence of Limbal Epithelial Progenitor/Stem Cells. *Stem Cells.* 2015;33(11):3341-55.
22. He H, Tan Y, Duffort S, Perez VL, and Tseng SC. In vivo downregulation of innate and adaptive immune responses in corneal allograft rejection by HC-HA/PTX3 complex purified from amniotic

membrane. *Invest Ophthalmol Vis Sci.* 2014;55(3):1647-56.

23. Ferrari LF, Khomula EV, Araldi D, and Levine JD. CD44 Signaling Mediates High Molecular Weight Hyaluronan-Induced Antihyperalgesia. *J Neurosci.* 2018;38(2):308-21.
24. Bonet IJM, Araldi D, Khomula EV, Bogen O, Green PG, and Levine JD. Mechanisms Mediating High-Molecular-Weight Hyaluronan-Induced Antihyperalgesia. *J Neurosci.* 2020;40(34):6477-88.
25. Bonet IJM, Staurengo-Ferrari L, Araldi D, Green PG, and Levine JD. Second messengers mediating high-molecular-weight hyaluronan-induced antihyperalgesia in rats with chemotherapy-induced peripheral neuropathy. *Pain.* 2022;163(9):1728-39.
26. Bonet IJM, Khomula EV, Araldi D, Green PG, and Levine JD. PI3Kgamma/AKT Signaling in High Molecular Weight Hyaluronan (HMWH)-Induced Anti-Hyperalgesia and Reversal of Nociceptor Sensitization. *J Neurosci.* 2021;41(40):8414-26.
27. He H, Zhang S, Tighe S, Son J, and Tseng SCG. Immobilized heavy chain-hyaluronic acid polarizes lipopolysaccharide-activated macrophages toward M2 phenotype. *J Biol Chem.* 2013;288(36):25792-803.
28. Cavanaugh DJ, Lee H, Lo L, Shields SD, Zylka MJ, Basbaum AI, and Anderson DJ. Distinct subsets of unmyelinated primary sensory fibers mediate behavioral responses to noxious thermal and mechanical stimuli. *Proc Natl Acad Sci U S A.* 2009;106(22):9075-80.
29. Tiwari V, Yang F, He SQ, Shechter R, Zhang C, Shu B, et al. Activation of Peripheral mu-opioid Receptors by Dermorphin [D-Arg2, Lys4] (1-4) Amide Leads to Modality-preferred Inhibition of Neuropathic Pain. *Anesthesiology.* 2016;124(3):706-20.
30. Domocos D, Follansbee T, Nguyen A, Nguyen T, Carstens MI, and Carstens E. Cinnamaldehyde elicits itch behavior via TRPV1 and TRPV4 but not TRPA1. *Itch (Phila).* 2020;5(3).
31. Janiszewska M, De Vito C, Le Bitoux MA, Fusco C, and Stamenkovic I. Transportin regulates nuclear import of CD44. *J Biol Chem.* 2010;285(40):30548-57.
32. Campo GM, Avenoso A, Micali A, Nastasi G, Squadrito F, Altavilla D, et al. High-molecular weight hyaluronan reduced renal PKC activation in genetically diabetic mice. *Biochim Biophys Acta.* 2010;1802(11):1118-30.
33. Dzwonek J, and Wilczynski GM. CD44: molecular interactions, signaling and functions in the nervous system. *Front Cell Neurosci.* 2015;9:175.
34. Protin U, Schweighoffer T, Jochum W, and Hilberg F. CD44-deficient mice develop normally with changes in subpopulations and recirculation of lymphocyte subsets. *J Immunol.* 1999;163(9):4917-23.
35. Zhang C, Hu MW, Wang XW, Cui X, Liu J, Huang Q, et al. scRNA-sequencing reveals subtype-specific transcriptomic perturbations in DRG neurons of Pirt(EGFPf) mice in neuropathic pain condition. *Elife.* 2022;11.
36. Vroman R, Hunter RS, Wood MJ, Davis OC, Malfait Z, George DS, et al. Analysis of matrisome expression patterns in murine and human dorsal root ganglia. *Front Mol Neurosci.* 2023;16:1232447.
37. Freeman SA, Vega A, Riedl M, Collins RF, Ostrowski PP, Woods EC, et al. Transmembrane Pickets Connect Cyto- and Pericellular Skeletons Forming Barriers to Receptor Engagement. *Cell.* 2018;172(1-2):305-17 e10.
38. Foger N, Marhaba R, and Zoller M. Involvement of CD44 in cytoskeleton rearrangement and raft reorganization in T cells. *J Cell Sci.* 2001;114(Pt 6):1169-78.
39. Fujiwara I, Zweifel ME, Courtemanche N, and Pollard TD. Latrunculin A Accelerates Actin Filament Depolymerization in Addition to Sequestering Actin Monomers. *Curr Biol.* 2018;28(19):3183-92 e2.
40. Witke W. The role of profilin complexes in cell motility and other cellular processes. *Trends Cell Biol.* 2004;14(8):461-9.
41. Alkam D, Feldman EZ, Singh A, and Kiaei M. Profilin1 biology and its mutation, actin(g) in disease. *Cell Mol Life Sci.* 2017;74(6):967-81.
42. Stevens SR, and Rasband MN. Ankyrins and neurological disease. *Curr Opin Neurobiol.* 2021;69:51-7.
43. Fehon RG, McClatchey AI, and Bretscher A. Organizing the cell cortex: the role of ERM proteins. *Nat Rev Mol Cell Biol.* 2010;11(4):276-87.

44. Vasilev F, Ezhova Y, and Chun JT. Signaling Enzymes and Ion Channels Being Modulated by the Actin Cytoskeleton at the Plasma Membrane. *Int J Mol Sci.* 2021;22(19).
45. Rogawski MA, and Loscher W. The neurobiology of antiepileptic drugs for the treatment of nonepileptic conditions. *Nat Med.* 2004;10(7):685-92.
46. Schroeder JE, and McCleskey EW. Inhibition of Ca2+ currents by a mu-opioid in a defined subset of rat sensory neurons. *J Neurosci.* 1993;13(2):867-73.
47. Garber K. Peptide leads new class of chronic pain drugs. *Nat Biotechnol.* 2005;23(4):399.
48. Green DP, Limjunyawong N, Gour N, Pundir P, and Dong X. A Mast-Cell-Specific Receptor Mediates Neurogenic Inflammation and Pain. *Neuron.* 2019;101(3):412-20 e3.
49. Stern R, Asari AA, and Sugahara KN. Hyaluronan fragments: an information-rich system. *Eur J Cell Biol.* 2006;85(8):699-715.
50. Qi L, Iskols M, Shi D, Reddy P, Walker C, Lezgiyeva K, et al. A mouse DRG genetic toolkit reveals morphological and physiological diversity of somatosensory neuron subtypes. *Cell.* 2024;187(6):1508-26 e16.
51. Renthal W, Tochitsky I, Yang L, Cheng YC, Li E, Kawaguchi R, et al. Transcriptional Reprogramming of Distinct Peripheral Sensory Neuron Subtypes after Axonal Injury. *Neuron.* 2020;108(1):128-44 e9.
52. Bonet IJM, Green PG, and Levine JD. Sexual dimorphism in the nociceptive effects of hyaluronan. *Pain.* 2021;162(4):1116-25.
53. Tseng SC. HC-HA/PTX3 Purified From Amniotic Membrane as Novel Regenerative Matrix: Insight Into Relationship Between Inflammation and Regeneration. *Invest Ophthalmol Vis Sci.* 2016;57(5):ORSFh1-8.
54. Yasuda M, Kido K, Ohtani N, and Masaki E. Mast cell stabilization promotes antinociceptive effects in a mouse model of postoperative pain. *J Pain Res.* 2013;6:161-6.
55. Pogatzki EM, and Raja SN. A mouse model of incisional pain. *Anesthesiology.* 2003;99(4):1023-7.
56. Feehan AK, and Zadina JE. Morphine immunomodulation prolongs inflammatory and postoperative pain while the novel analgesic ZH853 accelerates recovery and protects against latent sensitization. *J Neuroinflammation.* 2019;16(1):100.
57. Kabadi R, Kouya F, Cohen HW, and Banik RK. Spontaneous pain-like behaviors are more sensitive to morphine and buprenorphine than mechanically evoked behaviors in a rat model of acute postoperative pain. *Anesth Analg.* 2015;120(2):472-8.
58. Gao X, Han S, Huang Q, He SQ, Ford NC, Zheng Q, et al. Calcium imaging in population of dorsal root ganglion neurons unravels novel mechanisms of visceral pain sensitization and referred somatic hypersensitivity. *Pain.* 2021;162(4):1068-81.
59. Ford NC, Barpujari A, He SQ, Huang Q, Zhang C, Dong X, et al. Role of primary sensory neurone cannabinoid type-1 receptors in pain and the analgesic effects of the peripherally acting agonist CB-13 in mice. *Br J Anaesth.* 2022;128(1):159-73.

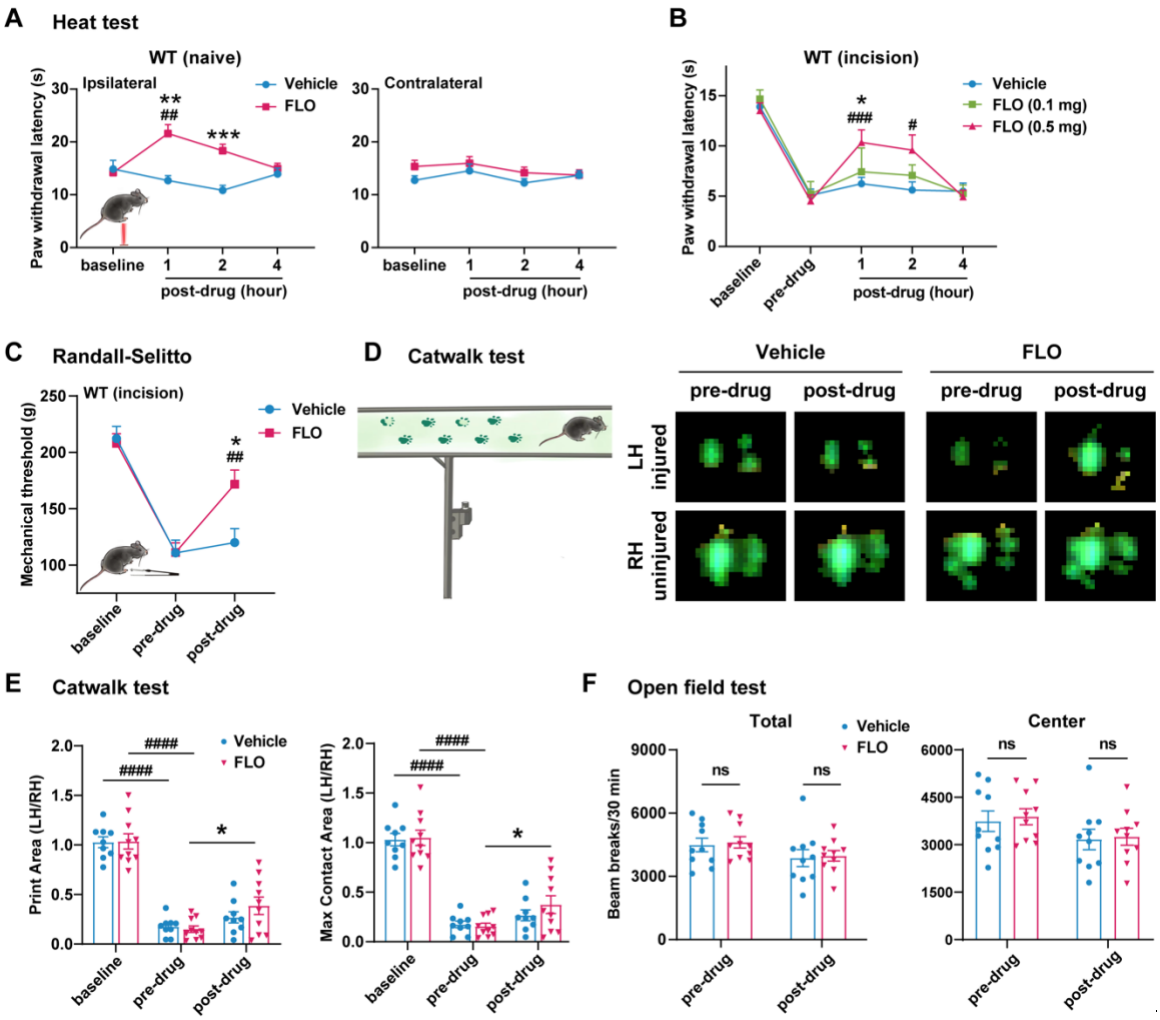

Figure 1. Intra-paw injections of FLO inhibited heat nociception in naive wild-type (WT) mice and attenuated both heat and mechanical hyperalgesia after the plantar-incision.

(A) Paw withdrawal latency (PWL) to heat stimulation in naïve WT mice before and after injection of FLO (0.5 mg, 20 µL) or the vehicle (saline, 20 µL) into the dorsum of the hind paw. Ipsilateral: injected side; Contralateral: un-injected side. N=10/group.

(B) The PWL ipsilateral to the side of plantar-incision was measured before and 1, 2, 4 hours after intra-paw injections of FLO (0.1 mg, 0.5 mg, 20 µL) or the vehicle in WT mice during Days 2-4 post-injury. N=7-13/group.

(C) The mechanical paw withdrawal threshold (PWT) to noxious pinch applied to the side of plantar-incision was measured before and 1 hour after intra-paw injection of FLO (0.5 mg, 20 µL) or vehicle with the Randall-Selitto test during Days 2-4 post-injury. N=10-11/group.

(D) Schematic of the Catwalk gait analysis (left) and the representative paw print images (right).

(E) Quantification of print area and maximum contact area in Catwalk test before and 1 hour after an intra-paw injection of FLO (0.5 mg, 20 µL) or vehicle on Day 2 post-injury. The left hind paw (LH) received the incision and drug treatment, and data were normalized to the right side (RH). N=9-10/group.

(F) Locomotor function and exploration were assessed in the open field test (30-min duration). The number of total, central and peripheral beam breaks were measured before and at 1 hour after an intra-paw injection of FLO (0.5 mg, 20 µL) or vehicle during Days 2-4 post-injury. N=10/group.

Data are mean ± SEM. Two-way mixed model ANOVA followed by Bonferroni post hoc test. (A-C) $^{*}P<0.05$, $^{**}P<0.01$, $^{***}P<0.001$ versus vehicle; $^{\#}P<0.05$, $^{\#\#}P<0.01$, $^{\#\#\#}P<0.001$ versus baseline (A) or pre-drug (B, C). (E, F) $^{*}P<0.05$, $^{**}P<0.01$ versus pre-drug; $^{\#\#\#}P<0.001$, $^{\#\#\#\#}P<0.0001$ versus baseline. ns = not significant.

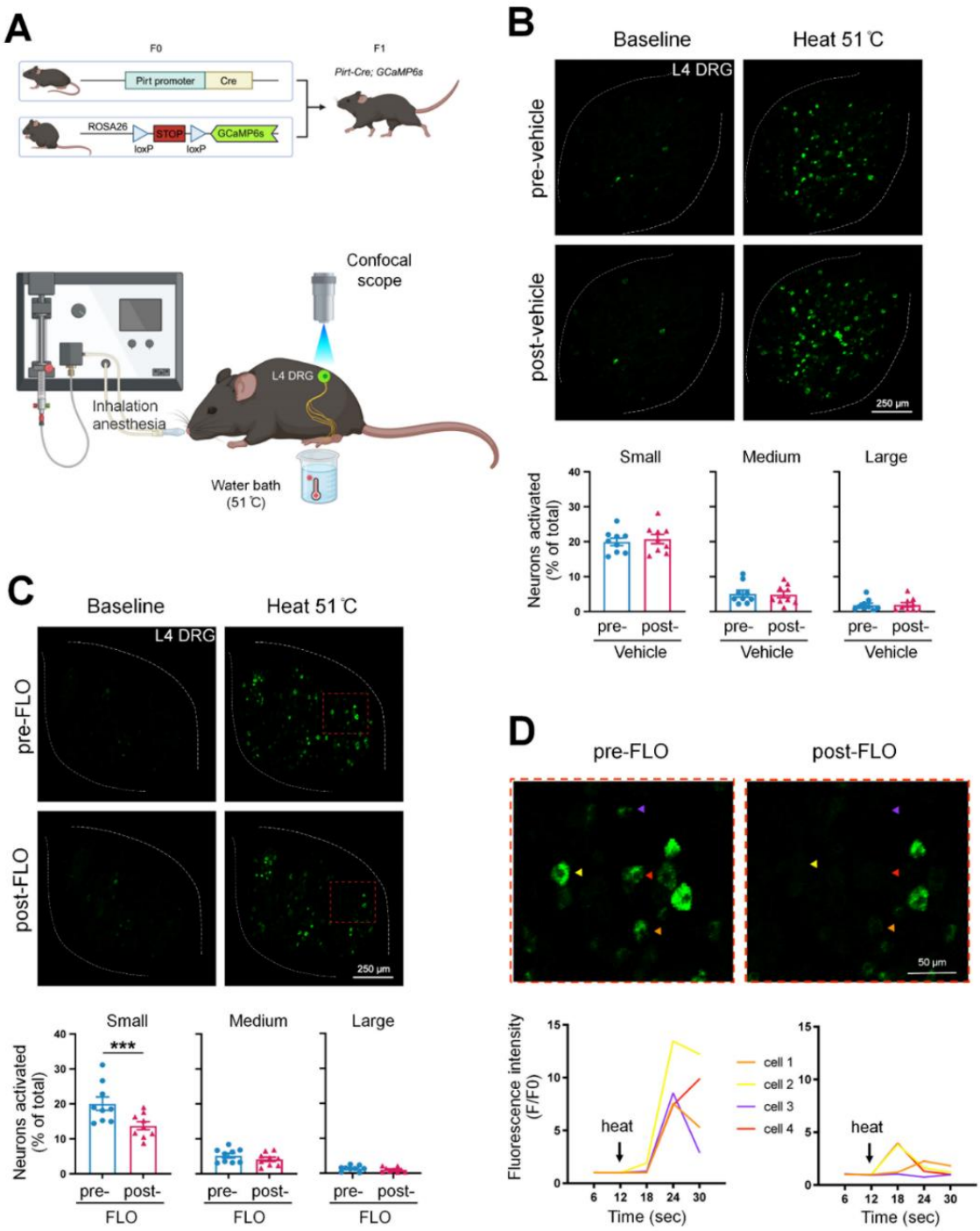

Figure 2. FLO acutely attenuated the responses of small DRG neurons to noxious heat stimulation.

(A) Upper: Strategy for generating *Pirt-Cre*; *GCaMP6s* mice. Lower: Schematic diagram illustrates the experimental setup for in vivo optical imaging of L4 DRG neurons and applying test stimulation.

(B-C) Upper: Representative images of calcium transients in DRG neurons in response to noxious heat stimulation (51°C water bath) applied to the hind paw before and 1 hour

after an intra-paw injection of vehicle (B, saline) or FLO (C, 0.5 mg, 20 μL) at Day 2 after plantar-incision. Lower: Percentages of small-, medium- and large-size neurons that were activated (ΔF/F ≥ 30%) by heat stimulation before and after vehicle or FLO. DRG neurons were categorized according to cell body size as <450 μm2 (small), 450–700 μm2 (medium), and >700 μm2 (large). N=9 /group.

(D) The higher-magnification representative images (upper) and calcium transient traces (lower) show increased fluorescence intensities in four DRG neurons (indicated by colored arrows) responding to heat stimulation, and decreased responses after FLO treatment.

Data are mean ± SEM. (B, C) Paired t-test. $^{***}P<0.001$ versus pre-drug.

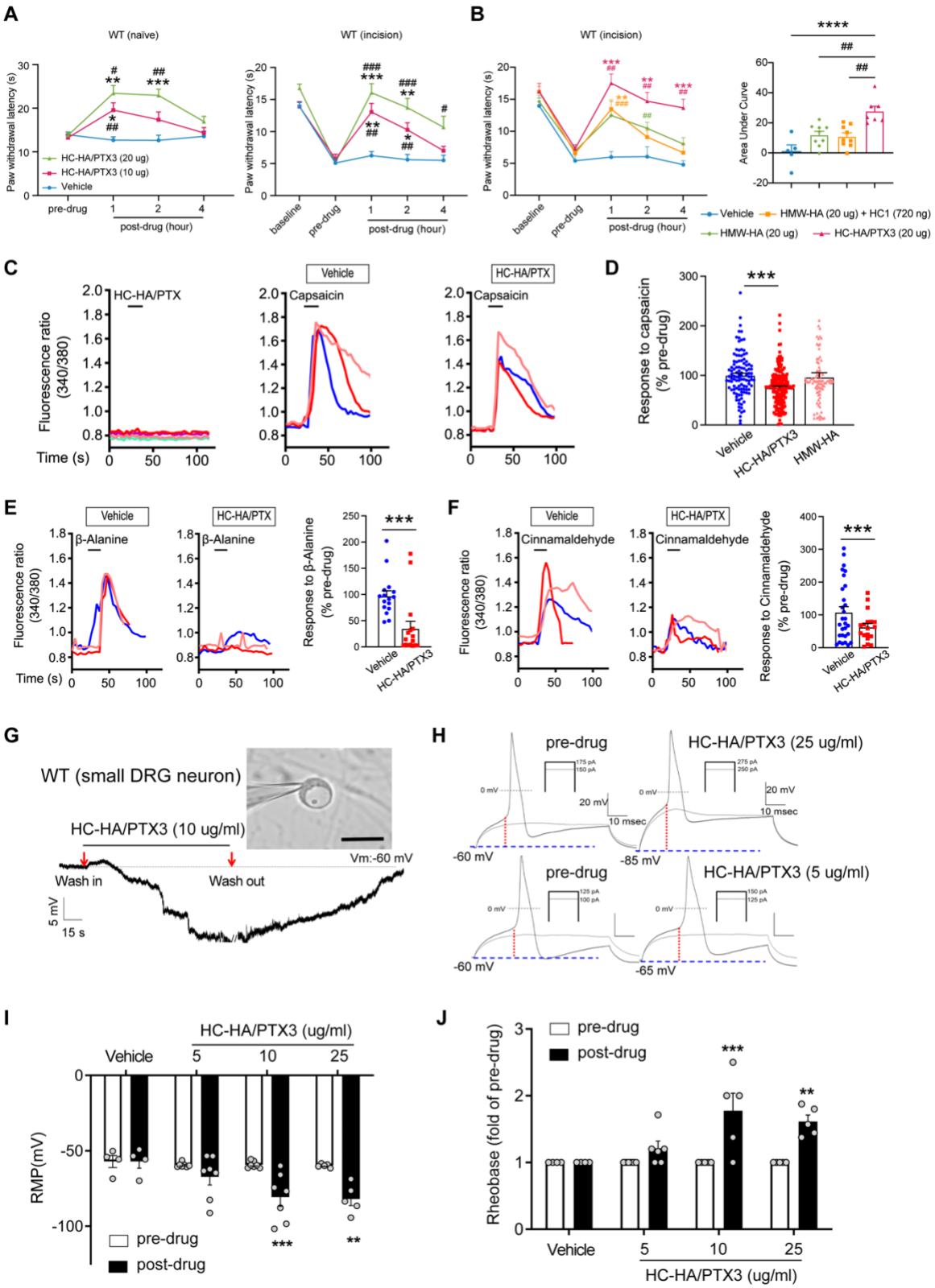

Figure 3. HC-HA/PTX3 inhibited heat hypersensitivity in wild-type (WT) mice after plantar-incision and attenuated DRG neuron activation.

(A) Left: intra-paw injection of HC-HA/PTX3 (10 μg or 20 μg, 20 μL), but not vehicle

(saline), increased paw withdrawal latency (PWL) to heat stimulation in naïve WT mice. N=8-11/group. Right: intra-paw injection of HC-HA/PTX3 (10 μg or 20 μg, 20 μL) dose-dependently attenuated the heat hypersensitivity during Days 2-4 after plantar-incision. N=9-16/group.
(B) Right: intra-paw injection of HC-HA/PTX3 (20 μg, 20 μL) showed superior anti-hyperalgesic effect compared to HMW-HA ((20 μg, 20 μL)) alone and the mixture of HMW-HA (20 μg) and HC1 (720 ng) during days 2-4 after plantar-incision. Left: analyzing the Area Under the Curve (AUC) to assess the anti-hyperalgesic effect of each group. N=5-9/group.
(C) HC-HA/PTX3 inhibited the calcium responses evoked by capsaicin (a TRPV1 agonist, 0.3 μM) in WT DRG neurons. HC-HA/PTX3 alone did not evoke $[Ca^{2+}]_i$ elevation. Pre-treatment (20 min) of HC-HA/PTX3 (15 μg/mL, bath application) reduced capsaicin-evoked $[Ca^{2+}]_i$ rising.
(D) The quantification of $[Ca^{2+}]_i$ rising evoked by capsaicin in DRG neurons pre-treated with the vehicle, HC-HA/PTX3 (15 μg/mL), or HMW-HA (15 μg/mL). N=109-170 neurons/group.
(E) Left: Traces show that the β-alanine (a MrgprD agonist, 1 mM) evoked an increase in $[Ca^{2+}]_i$, which was also inhibited by HC-HA/PTX3. Right: The quantification of evoke $[Ca^{2+}]_i$ rising by β-alanine. N=10-25 neurons/group.
(F) Left: Traces show that cinnamaldehyde (a TRPA1 agonist, 1 mM) evoked an increase in $[Ca^{2+}]_i$, which was inhibited by HC-HA/PTX3. Right: The quantification of evoke $[Ca^{2+}]_i$ rising by cinnamaldehyde. N=15-35 neurons/group.
(G) An example trace of membrane potential (Vm) which changed from resting level (-60 mV) toward a more hyperpolarized state after HC-HA/PTX3 (10 μg/mL) in a small DRG neuron (insert, scale bar: 25 μm). Vm returned to pre-drug level after washout. DRG neurons were categorized according to cell body diameter as <20 μm (small), 20–30 μm (medium), and >30 μm (large).
(H) Example traces of action potentials (APs) evoked by injection of current in small DRG neurons 5 min after bath application of vehicle or HC-HA/PTX3 (5, 25 μg/mL).
(I) HC-HA/PTX3 concentration-dependently altered the intrinsic membrane properties of small DRG neurons. Quantification of the resting membrane potential (RMP) before and at 5 min after bath application of vehicle or HC-HA/PTX3 (5, 10, 25 μg/mL). N=4-7/group.
(J) Quantification of rheobase in small DRG neurons at 5 min after vehicle or HC-HA/PTX3. The rheobase after drug was normalized to pre-drug value. N=5-7/group.
Data are mean ± SEM. (A, B: right) Two-way mixed model ANOVA followed by Bonferroni post hoc test. $^{*}P< 0.05$, $^{**}P<0.01$, $^{***}P<0.001$ versus vehicle; $^{\#}P<0.05$, $^{\#\#}P<0.01$, $^{\#\#\#}P<0.001$ versus pre-drug. (B: left, C) One-way ANOVA followed by Bonferroni post hoc test. $^{***}P<0.001$ versus vehicle; $^{\#\#}P<0.01$ versus other groups. (E, F) Paired t-test. $^{***}P<0.001$ versus vehicle. (I, J) Two-way mixed model ANOVA followed by Bonferroni post hoc test. $^{*}P<0.05$, $^{**}P<0.01$ versus pre-drug.

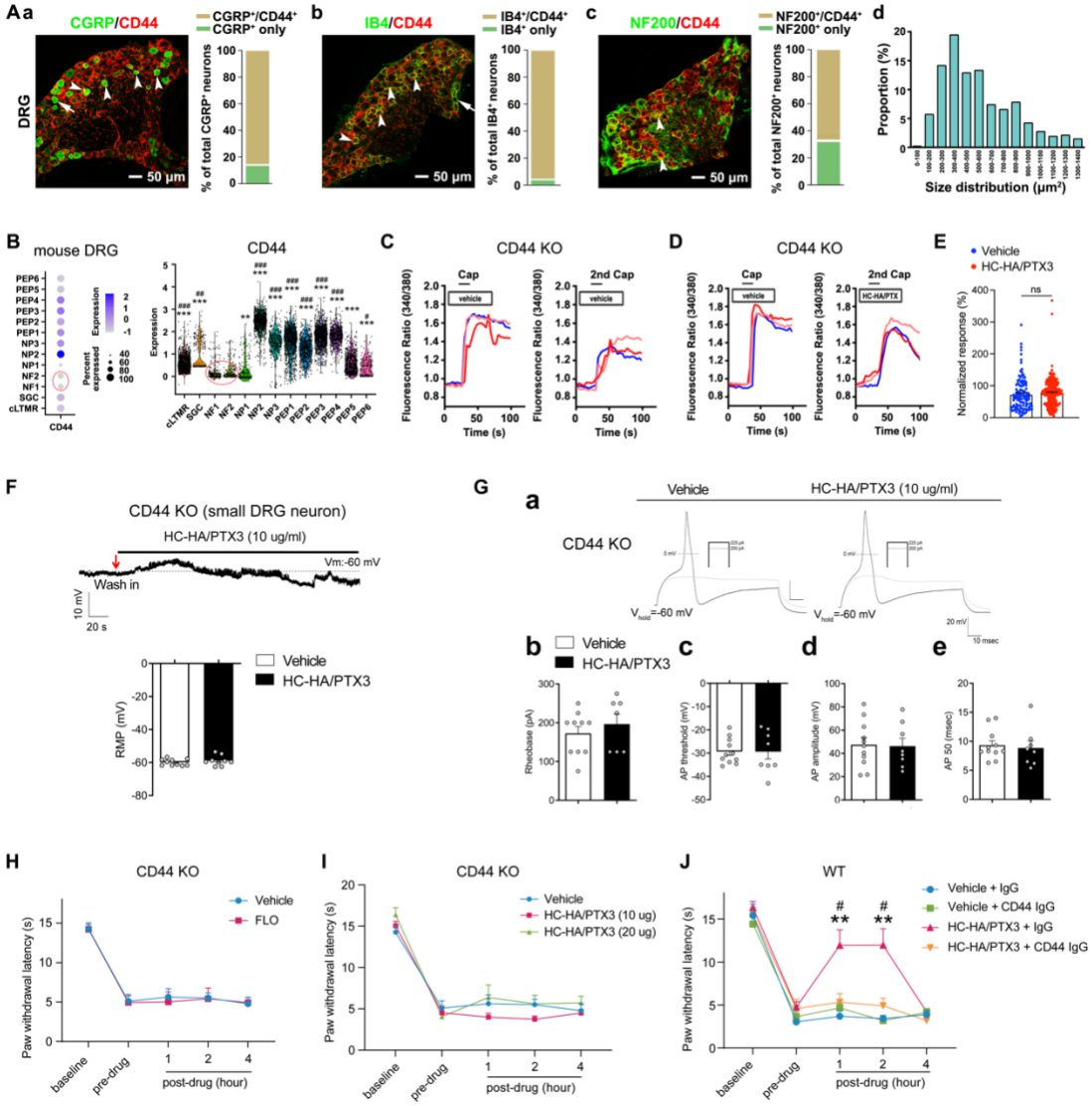

Figure 4. FLO and HC-HA/PTX3 inhibited pain via CD44-dependent mechanisms.
(A) The expression of CD44 in the DRG of wild-type (WT) mice. Left: Colocalization of CD44 and CGRP (a), IB4 (b) and NF200 (c) immunoreactivity (IR). Right: The quantification of CD44-expressing neurons (as % of total neurons in each subpopulation, $IB4^+$: 96%; $CGRP^+$: 82%; $NF200^+$: 68%, N=4) (d) The size distribution of CD44-expressing neurons.
(B) Left: Dot plot of CD44 gene expression in different clusters [SGC (1), NF (2), NP (3), PEP (6), cLTMR (1)] of DRG cells from WT mice in single-cell RNA-sequencing study. The dot size represents the percentage of cells expressing CD44, and the color scale indicates the average normalized expression level. The NF1 and NF2 clusters were indicated with a red circle. Right: Violin plot shows the CD44 expression levels in each cluster. SGC: satellite glial cells; NF, Aβ or Aδ low-threshold mechanoreceptors or proprioceptors; NP, non-peptidergic nociceptors or pruriceptors; PEP, peptidergic nociceptors; C-LTMR, C-fiber low-threshold mechanoreceptors. One-way ANOVA followed by Bonferroni post hoc test. $^{**}P<0.01$ $^{***}P<0.001$ versus NF1; $^{\#}P<0.05$, $^{\#\#}P<0.01$, $^{\#\#\#}P<0.001$ versus NF2.

(C) Traces show that the capsaicin (0.3 μM) evoked an increase of $[Ca^{2+}]_i$ in a small neuron from CD44 KO mouse. Compared to $[Ca^{2+}]_i$ rising evoked by the 1st capsaicin application, there was a reduction of $[Ca^{2+}]_i$ rising to the 2nd treatment, indicating TRPV1 desensitization. DRG neurons were categorized according to cell body diameter as <20 μm (small), 20–30 μm (medium), and >30 μm (large).
(D) Capsaicin-evoked increases of $[Ca^{2+}]_i$ before and after treatment (20 min) with HC-HA/PTX3 (10 μg/mL) in small DRG neurons from CD44 KO mice.
(E) The quantification of evoked $[Ca^{2+}]_i$ rising by capsaicin. HC-HA/PTX3 pretreatment did not reduce capsaicin-evoked $[Ca^{2+}]_i$ rising in CD44 KO neurons. N=100-120 neurons/group.
(F) HC-HA/PTX3 did not change the intrinsic membrane property of small DRG neurons from CD44 KO mice. Upper: An example trace of membrane potential (Vm) which remained around resting level (-60 mV) after HC-HA/PTX3 (10 μg/mL). Lower: Quantification of the resting membrane potential (RMP) at 5 min after vehicle (saline) and HC-HA/PTX3 (P=0.48).
(G) Upper: Examples traces of action potentials and rheobase evoked by injection of current in a small CD44 KO DRG neuron at 5 min after vehicle or HC-HA/PTX3 (10 μg/mL). Lower: Quantification of the rheobase levels (P=0.2), action potential (AP) threshold (P = 0.87), AP amplitude (P=0.75) and duration (P=0.82) in small DRG neurons from CD44 KO mice. N=7-11/group.
(H) Paw withdrawal latency (PWL) that was ipsilateral to the side of plantar-incision before and after an intra-paw injection of FLO (0.5 mg, 20 μL) or vehicle (saline, 20 μL) in CD44 KO mice (H, N=8-9/group) after plantar-incision.
(I) The ipsilateral PWL before and after an intra-paw injection of HC-HA/PTX3 (10 μg or 20 μg, 20 μL) or vehicle in CD44 KO mice after plantar-incision. N=7-9/group.
(J) The ipsilateral PWL before and after intra-paw injection of vehicle + control IgG, vehicle + CD44 IgG, HC-HA/PTX3 (10 μg) + control IgG or HC-HA/PTX3 (10 μg) + CD44 IgG (all IgG at 10 μg, 10 μL) in WT mice after plantar-incision. N=8-11/ group. Data are mean ± SEM. (E) One-way ANOVA followed by Bonferroni post hoc test. $^{*}P<0.05$ versus WT vehicle. ns=not significant. (F, G) Student's t-test. (H-K) Two-way mixed model ANOVA followed by Bonferroni post hoc test. $^{**}P<0.01$ versus vehicle or saline + IgG; $^{\#}P<0.05$ versus pre-drug.

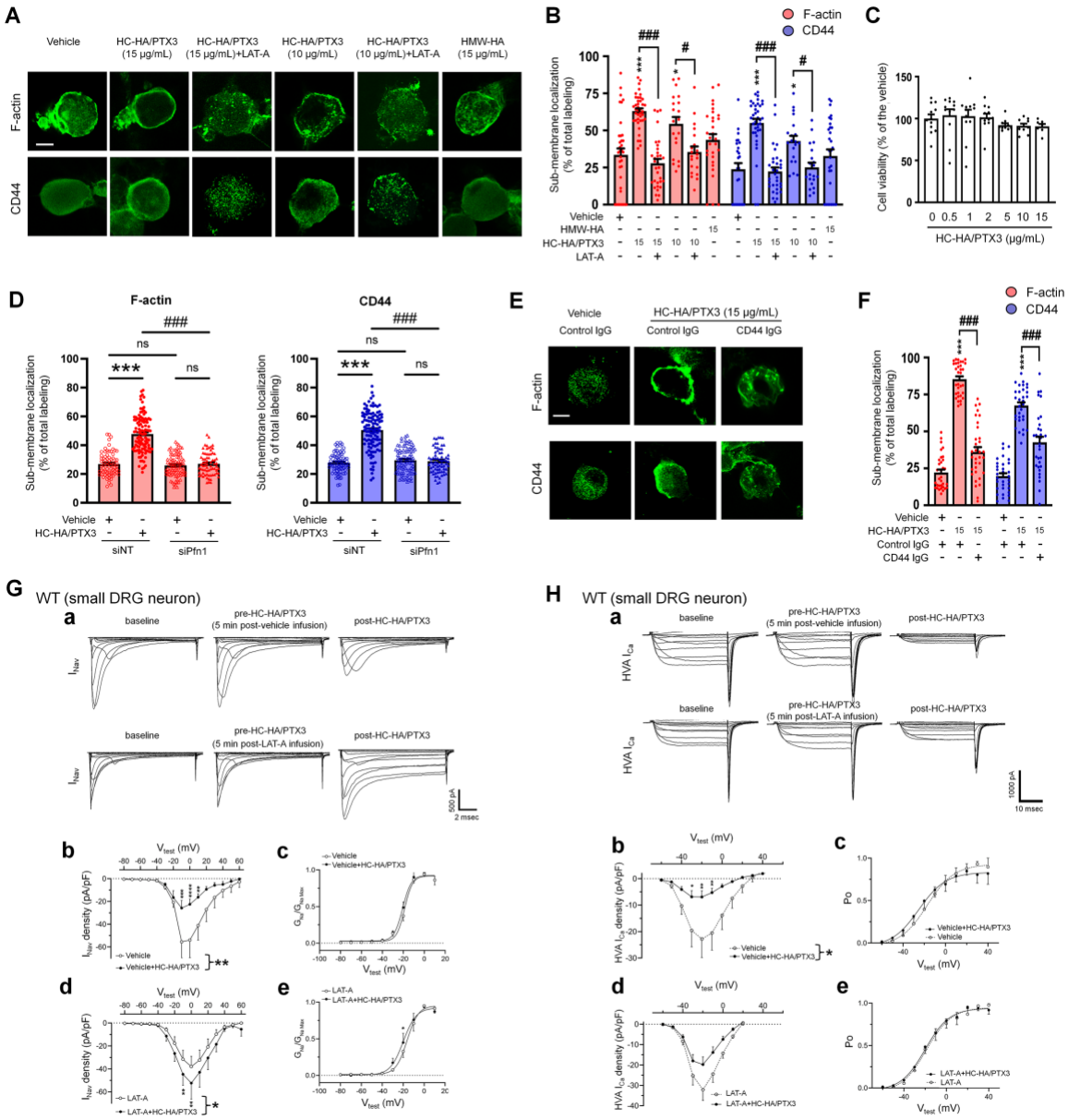

Figure 5. HC-HA/PTX3 induced cytoskeletal rearrangement which contributes to its inhibition of I_{Nav} and HVA I_{Ca}.

(A) Example images show the distribution of F-actin and CD44 staining in small DRG neurons of wild-type (WT) mice. Neurons were treated with bath application of vehicle (saline), HMW-HA (15 μg/mL), HC-HA/PTX3 (10, 15 μg/mL), or HC-HA/PTX3 (10, 15 μg/mL) combined with Latrunculin A (LAT-A, 1 μM) for 45 min. Scale bar: 5 μm. DRG neurons were categorized as <20 μm (small), 20–30 μm (medium), and >30 μm (large).

(B) Quantification of submembranous F-actin polymerization and translocation of CD44 in small WT DRG neurons after drug treatment. N=30-80/group.

(C) Proliferation MTT assay showed a lack of neuronal toxicity from 0.5, 1, 2, 5, 10, 15 μg/mL HC-HA/PTX3, compared to vehicle (100% viable cells). N=6-12 repetitions/group.

(D) Quantification of submembranous F-actin polymerization and translocation of CD44

in small DRG neurons. DRG neurons were electroporated with siRNA targeting Pfn1 (siPfn1) or non-targeting siRNA (siNT, control). Neurons were treated with vehicle (saline) or HC-HA/PTX3 (10 μg/mL) for 45 min. N=70-111/group.
(E) Changes in the submembrane distribution of F-actin and CD44 in WT DRG neurons treated with vehicle + control IgG (2 μg/mL), HC-HA/PTX3 (15 μg/mL) + control IgG (2 μg/mL), or HC-HA/PTX3 (15 μg/mL) + CD44 IgG (2 μg/mL) for 45 min. Scale bar: 5 μm.
(F) Quantification of the submembrane F-actin and CD44 labeling in each group.
(G) Infusion of LAT-A attenuated the inhibition of I_{Nav} by HC-HA/PTX3 in WT DRG neurons. a. Representative traces of I_{Nav} after 5 min infusions of vehicle (top row) or LAT-A (bottom row, 0.5 nM) through the recording electrode, followed by bath application of HC-HA/PTX3 (10 μg/mL). Lumbar DRG neurons were harvested on day 2-3 after plantar-incision. b. There was a significant interaction between the variation produced by HC-HA/PTX3 (10 μg/mL) and test voltages (V_{Test}) applied in vehicle-infused neurons, resulting in an overall I_{Nav} inhibition ($F(14,90) = 3.29$, ***$P<0.001$), and significantly decreased I_{Nav} density (pA/pF) from V_{Test} = -10 mV to +10 mV, as compared to pre-HC-HA/PTX3 treatment. N=7/group. c. HC-HA/PTX3 did not alter G_{Na}/G_{Na} max across the test voltages ($F(9,60) = 0.44$, $P=0.9$) in vehicle-infused neurons. N=7/group. d. There was a significant interaction between the variation produced by HC-HA/PTX3 (10 μg/mL) and V_{Test} applied in LAT-A-infused neurons, resulting in overall I_{Nav} increase ($F(14,120) = 1.87$, *$P<0.05$) and increased I_{Nav} density (pA/pF) from V_{Test} = -10 mV to 0 mV, as compared to pre-HC-HA/PTX3. N=9/group. e. HC-HA/PTX3 significantly increased the G_{Na}/G_{Na} max at V_{Test}= -20 mV in LAT-A-infused neurons (*$P<0.05$, N=9/group).
(H) LAT-A attenuated the inhibition of HVA-I_{Ca} by HC-HA/PTX3 in WT DRG neurons. a. Representative traces of HVA-I_{Ca} in small WT DRG neurons after 5 min infusions of vehicle (top row) or LAT-A (bottom row, 0.5 nM), followed by bath application of HC-HA/PTX3 (10 μg/mL). b. In vehicle-infused neurons, HC-HA/PTX3 (10 μg/mL) significantly decreased HVA-I_{Ca} ($F(1,12)=6.52$, *$P=0.02$) and HVA-I_{Ca} conductance (I/Imax) from V_{Test} = -40 mV to +10 mV, as compared to pre-HC-HA/PTX3. N = 7. c. HC-HA/PTX3 did not alter the channel open probability (Po) in vehicle-infused neurons ($P=0.82$, N=7). d. In LAT-A-infused neurons, HC-HA/PTX3 only modestly reduced HVA-I_{Ca} conductance across test voltages applied ($F(1,12)=0.27$, $P=0.6$, N=8). e. HC-HA/PTX3 did not alter Po in LAT-A-infused neurons ($P=0.94$, N=8).
Data are mean ± SEM. (B, C, D, F) One-way ANOVA followed by Bonferroni post hoc test. *$P< 0.05$, ***$P<0.001$ versus vehicle; #$P<0.05$, ###$P<0.001$ versus indicated group. (G, H) Two-way repeated measures ANOVA with Holm-Sidak post-test. *$P< 0.05$, **$P< 0.01$, ***$P<0.001$, ****$P<0.0001$ versus vehicle infusion or LAT-A infusion group.

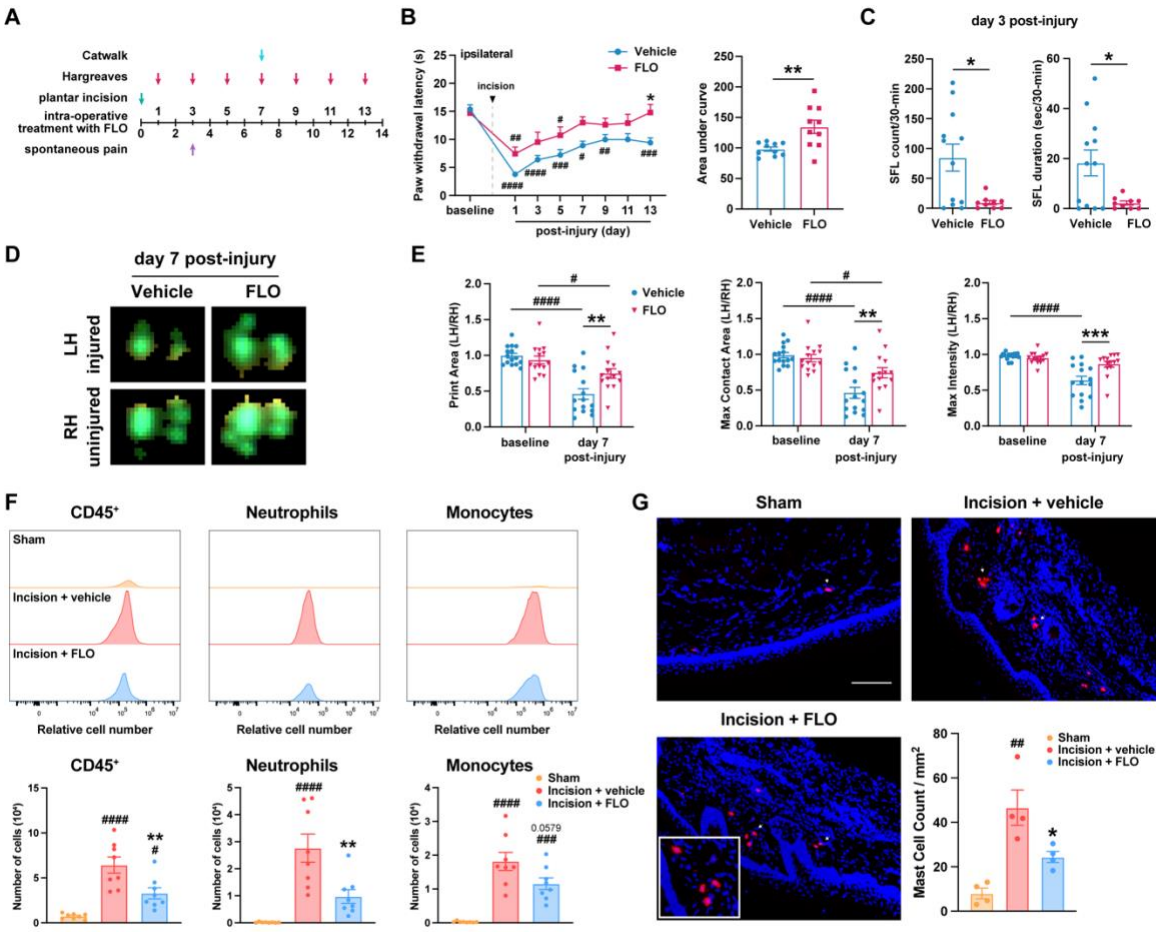

Figure 6. An intra-operative FLO treatment reduced local immune cell recruitment after plantar-incision and attenuated the development of post-surgical pain.

(A) The schematic diagram of the experimental protocol. FLO or vehicle (saline) was intra-operatively applied to the plantar-incision site during surgery.

(B) Left: The ipsilateral paw withdrawal latency (PWL) to radiant heat stimulation before and at days 1-13 after plantar incision in wild-type (WT) mice that received an intra-operative FLO (1 mg) or vehicle treatment. Right: The area under the curve (AUC) for PWL. N=10/group.

(C) The spontaneous foot lifting (SFL) count and the SFL duration were measured at Day 3 post-injury in WT mice that received an intra-operative treatment of FLO (1 mg) or vehicle. N=9-12/group.

(D) Representative paw print images in Catwalk test.

(E) Quantification of print area, maximum contact area, and maximum intensity (left hind paw normalized to right hind paw) before and at Day 7 post-injury in WT mice treated with an intra-operative FLO (1 mg) or vehicle. N=14-15/group

(F) Upper: Representative fluorescence histograms of $CD45^+$ cells, $CD11b^+Ly6G^+$ neutrophils, and $CD11b^+Ly6G^-Ly6C^+$ monocytes in biopsies from hind paw skin in WT mice at 24 hours after sham surgery, plantar-incision topically treated with vehicle or

FLO (1 mg). Lower: The quantification of absolute number of $CD45^+$ cells, $CD11b^+Ly6G^+$ neutrophils, and $CD11b^+Ly6G^-Ly6C^+$ monocytes. N=8/group.
(G) Upper: Examples of fluorescence microscope images of plantar skin sections of *Mrgprb2-Cre tdT* mice at 24 hours after sham surgery, plantar-incision treated with an intra-operative vehicle or FLO (1 mg). *Mrgprb2-Cre tdT*$^+$ mast cells were identified with red fluorescence (arrowheads). Scale bar: 100 μm. Lower: Mast cell counts per mm2 were compared between three groups. N=4/group.
Data are mean ± SEM. (B, E) Two-way mixed model ANOVA followed by Bonferroni post hoc test (left). Student's t-test (right). $^*P<0.05$, $^{**}P<0.01$, $^{***}P<0.001$ versus vehicle; $^{\#}P<0.05$, $^{\#\#}P<0.01$, $^{\#\#\#}P<0.001$, $^{\#\#\#\#}P<0.0001$ versus baseline. (C) Student's t-test. $^*P<0.05$ versus vehicle. (F, G) One-way ANOVA followed by Bonferroni post hoc test. $^{\#}P<0.05$, $^{\#\#}P<0.01$, $^{\#\#\#}P<0.001$, $^{\#\#\#\#}P<0.0001$ versus sham; $^*P<0.05$, $^{**}P<0.01$ versus incision + vehicle.

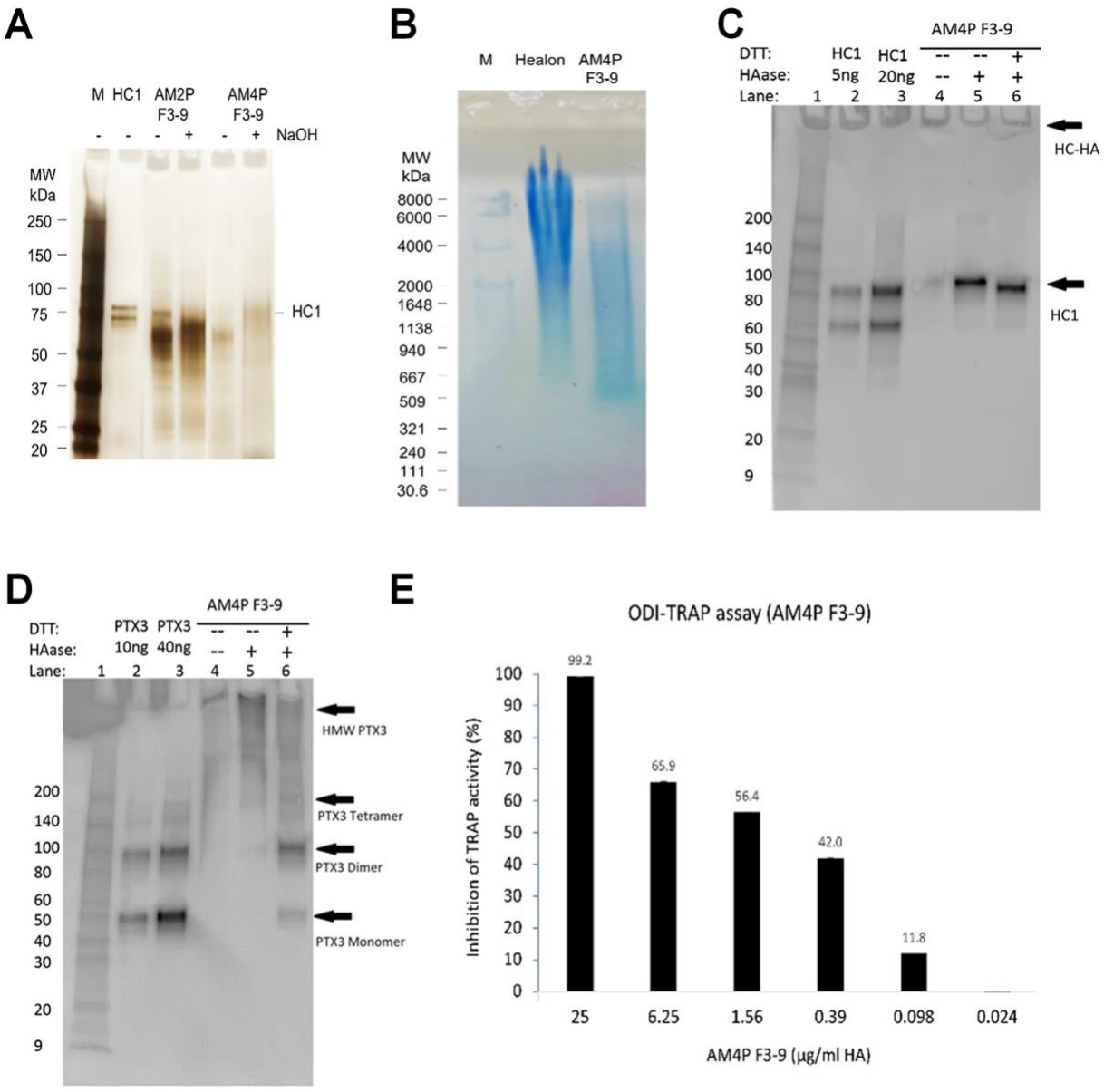

Fig. S1. Purification and characterization of HC-HA/PTX3.
(A) HC-HA/PTX3 was prepared from the human amniotic membrane by 2 runs (AM2P F3-9) or 4 runs (AM4P F3-9) of CsCl/4 M GnHCl ultracentrifugation and was then analyzed by silver staining. Each lane was loaded with 0.25 μg of HA without or with 100 mM NaOH treatment (25°C, 1 h) to cleave the bond between HA and HC1. (B) HC-HA/PTX3 (AM4P F3-9) purified from the amniotic membrane was electrophoresed on 0.5% agarose gel and stained with All-stains dye. Healon as a high-molecular-weight (HMW) HA control and HC-HA/PTX3 were loaded at 10 μg HA/lane; M: HA molecular weight ladder. (C-D) HC1 and PTX3 in HC-HA/PTX3 were detected by western blot using respective antibodies without (-) or with (+) hyaluronidase (HAase) treatment to release HC1 or HMW-PTX3, of which the latter can then be resolved into dimer or monomer without (-) or with (+) reduction with DTT. (E) Cloned murine RAW264.7

monocytes were seeded at 1x104 cells/cm2 in MEM α/10% FBS and differentiated into multi-nucleated osteoclasts with 25 ng/ml RANKL as the positive control and treated with HC-HA/PTX3 at different concentrations (0.024 – 25 μg/mL) for 3 days. The inhibition of TRAP activity in cell lysates was calculated as a percentage (%) of that of the positive control (shown on the top of each bar).

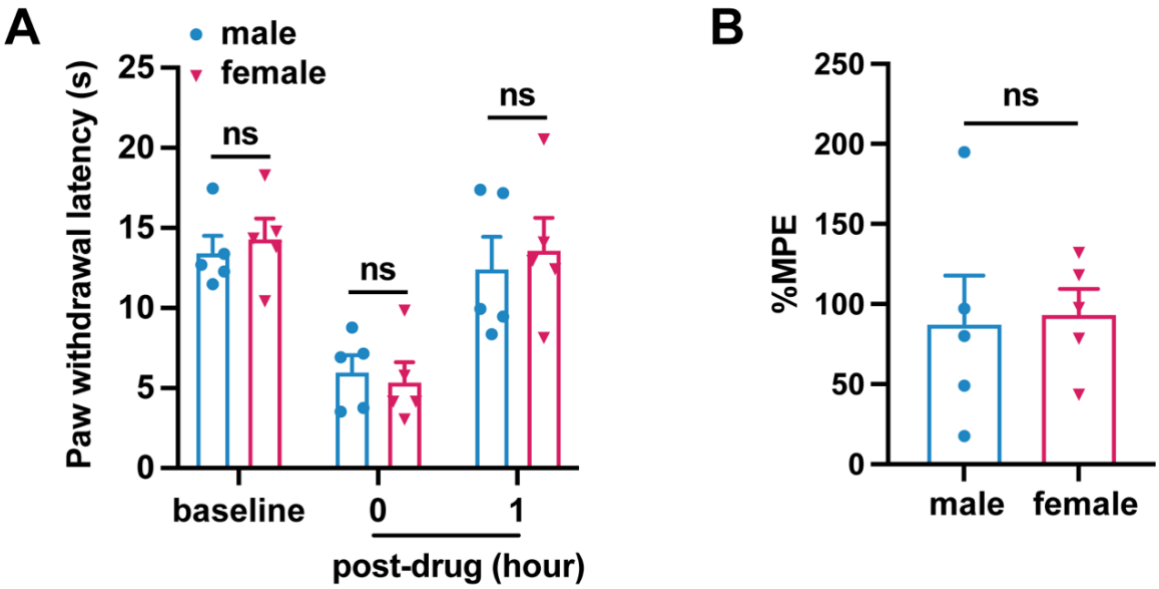

Fig. S2. HC-HA/PTX3 induced comparable inhibition of heat hyperalgesia in male and female mice after plantar incision.

(A) Paw withdrawal latency at different time point of male and female mice included in Figure 3B. (N= 5/sex) (B) The percentage of maximal possible effects (%MPE) at 1 hour post-drug were calculated for male and female mice included in Figure 3B. %MPE=1 - (baseline - post-drug) / (baseline - pre-drug). Data are mean ± SEM. (A) Two-way mixed model ANOVA followed by Bonferroni post hoc test. $^{*}P<0.05$ versus male. (B) Unpaired t-test.

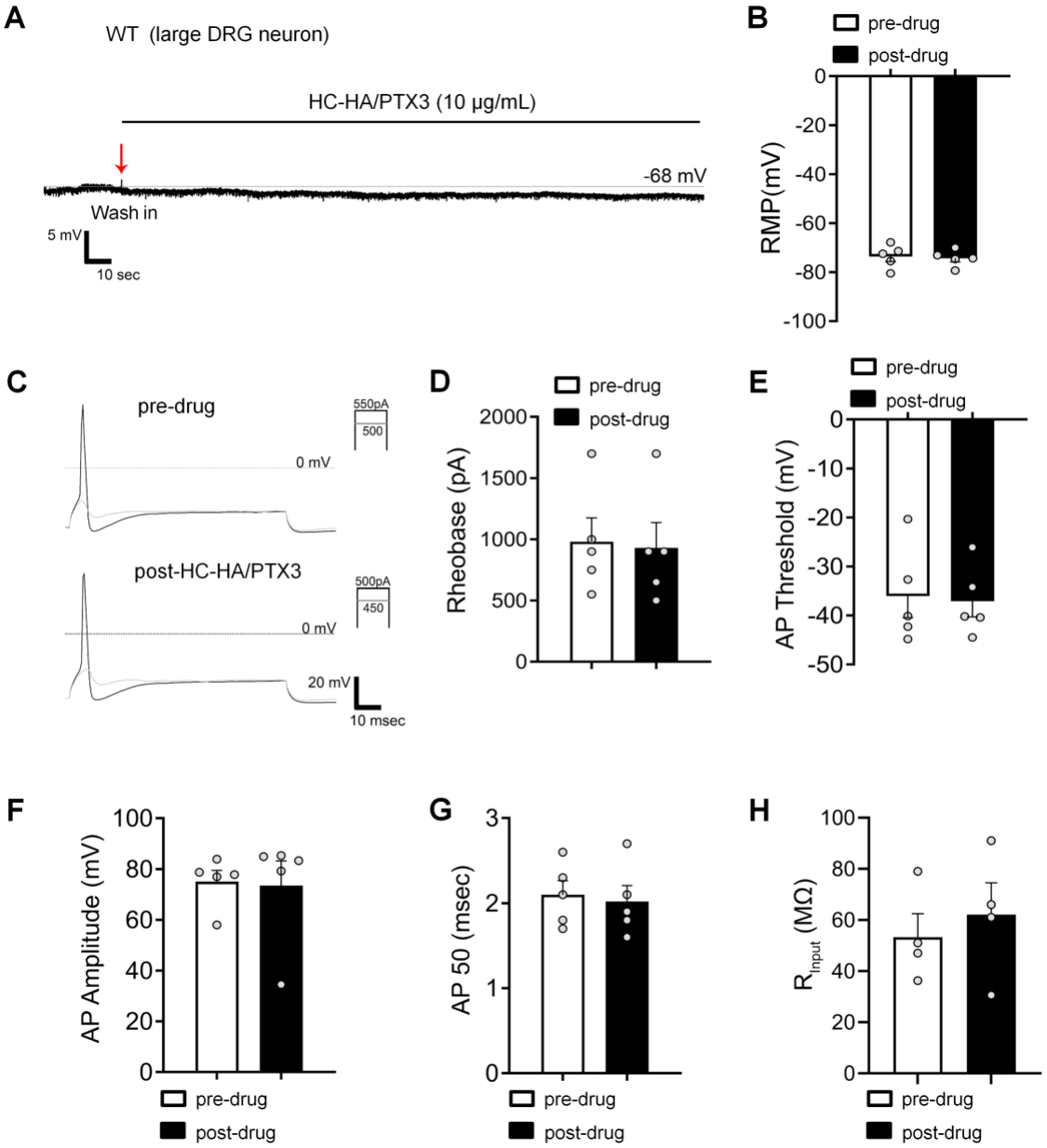

Fig. S3. HC-HA/PTX3 did not affect the excitability of large-diameter DRG neurons in wild-type (WT) mice after the plantar incision.

(A) The representative trace of membrane potential recorded under current-clamp conditions before and after HC-HA/PTX3 (15 µg/mL) treatment in a large DRG neuron of WT mice. Neurons were categorized according to cell body diameter as <20 µm (small), 20–30 µm (medium), and >30 µm (large). (B) The resting membrane potential (RMP) in large DRG neurons was not significantly changed at 5 min after HC-HA/PTX3 (10 µg/mL) treatment, compared to pre-drug (P=0.41). N=5. (C) Representative traces of rheobase measurements before and after HC-HA/PTX3 (10 µg/mL). (D-H) Quantification of the rheobase (D, P=0.09), action potential (AP) threshold (E, P=0.78), AP amplitude (F, P=0.8), AP duration (G, P=0.41), and the mean input resistance (Rinput, H, P=0.17) before and at 5 min after HC-HA/PTX3 (10 µg/mL) treatment. N=5. Data are

presented as mean ± SEM. (B, D-H) Paired t-test.

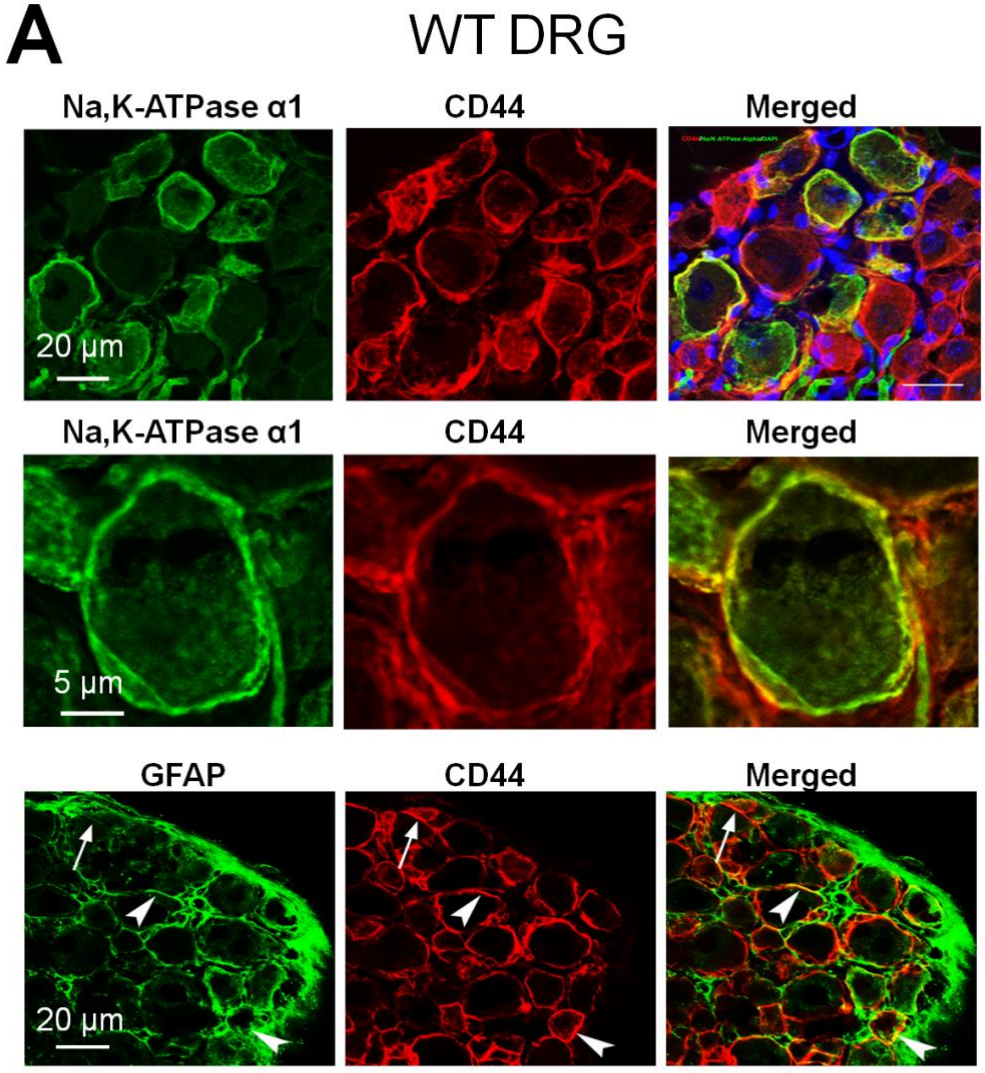

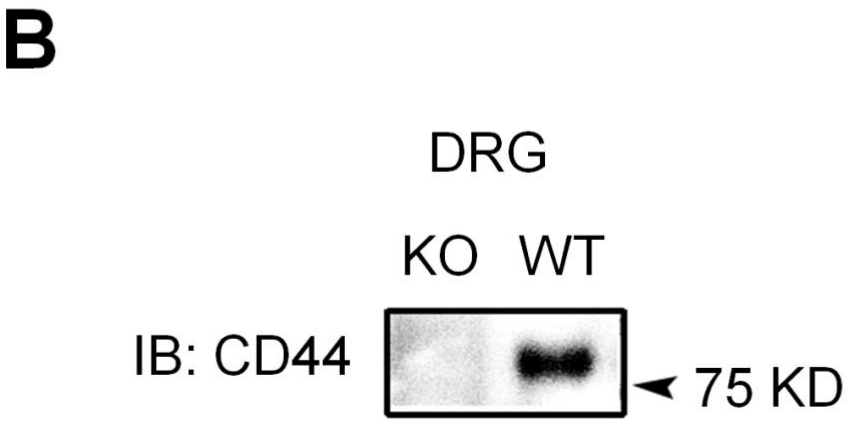

Fig. S4. The expression of CD44 in mouse DRG.
(A) Upper: Colocalization of CD44 and Na, K-ATPase alpha1 (a neuronal marker) immunoreactivity (IR) in wild-type (WT) mouse DRG. Blue: DAPI. Middle: A higher power view of CD44 and Na, K-ATPase alpha1 colocalization. Lower: Colocalization of CD44 and GFAP (a satellite glial cell marker) in DRG. Arrow: single-labeled cell; Arrowhead: double-labeled cell. (B) The specific CD44 band was not observed in the protein extracts derived from DRG tissues of CD44 knockout (KO) mice in the western blot study.

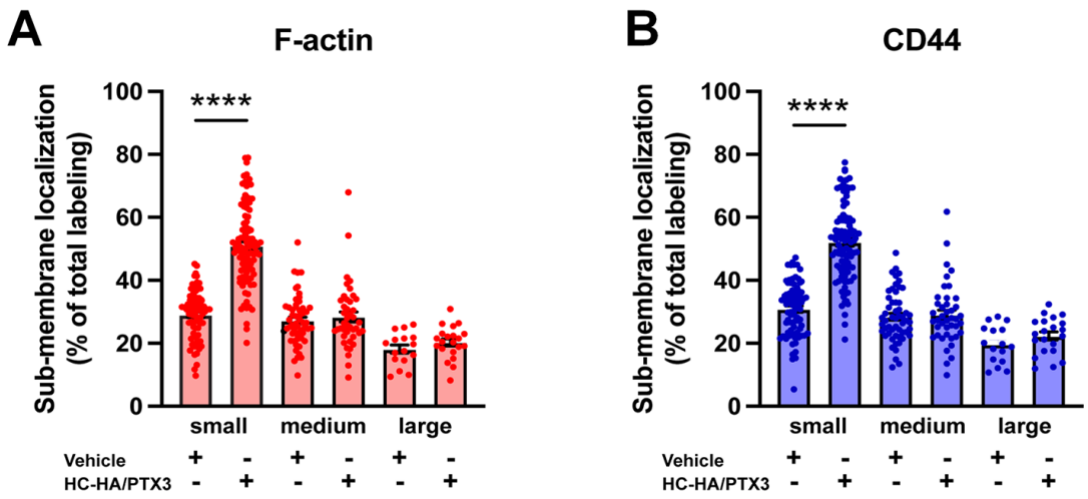

Fig. S5. Differential effects of HC-HA/PTX3 on sub-membranous F-actin polymerization and translocation of CD44 in small-, medium-, and large-diameter wild-type (WT) DRG neurons.

(A) Quantification of sub-membranous F-actin polymerization and (B) translocation of CD44 in different sizes of WT DRG neurons after HC-HA/PTX3 (10 μg/mL) or the vehicle (saline) treatment. DRG neurons were categorized according to cell body diameter as <20 μm (small), 20–30 μm (medium), and >30 μm (large). HC-HA/PTX3 increased sub-membranous F-actin polymerization and translocation of CD44 exclusively in small neurons. N=16-91/group. Data are mean ± SEM. One-way ANOVA followed by Bonferroni post hoc test. ****P< 0.0001 versus vehicle.

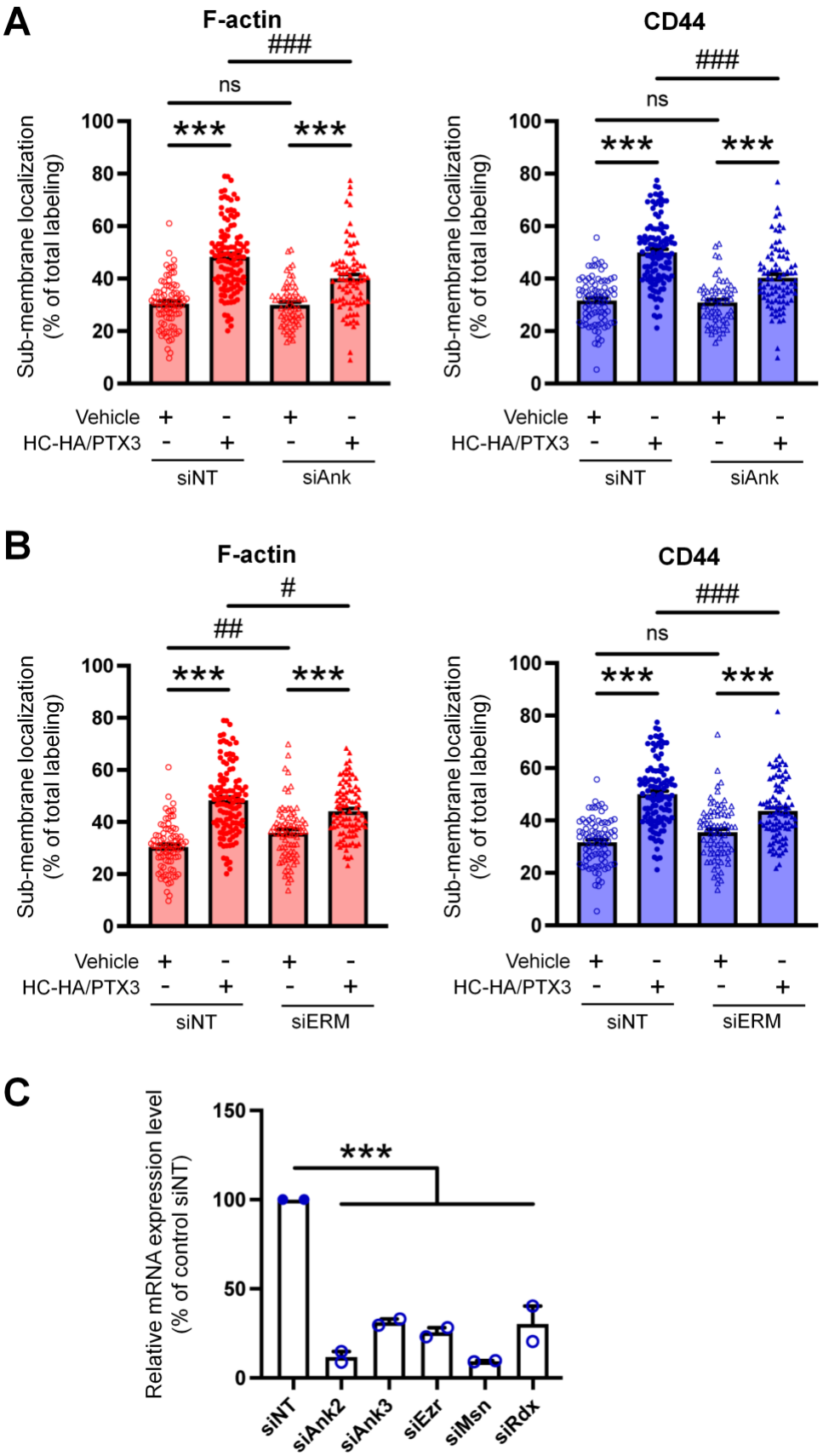

Fig. S6. Quantification of submembranous F-actin polymerization and translocation of CD44 in small-diameter wild-type (WT) DRG neurons in each group.
(A) DRG neurons were electroporated with siRNAs specifically targeting *Ank2* and *Ank3* (siAnk), (B) and those targeting *Ezr*, *Rdx*, and *Msn* (siERM) complex. Neurons were treated with a bath application of vehicle (saline) or HC-HA/PTX3 (10 μg/mL) for 45 min. N=59-114/group. (C) The mRNA expression of *Ank2*, *Ank3*, *Ezr*, *Msn*, and *Rdx* in DRG neurons electroporated with specific siRNAs were assayed by qPCR. N=2. Data are mean ± SEM. One-way ANOVA followed by Bonferroni post hoc test. ***P<0.001 versus vehicle; $^{###}$P<0.001 versus indicated group.

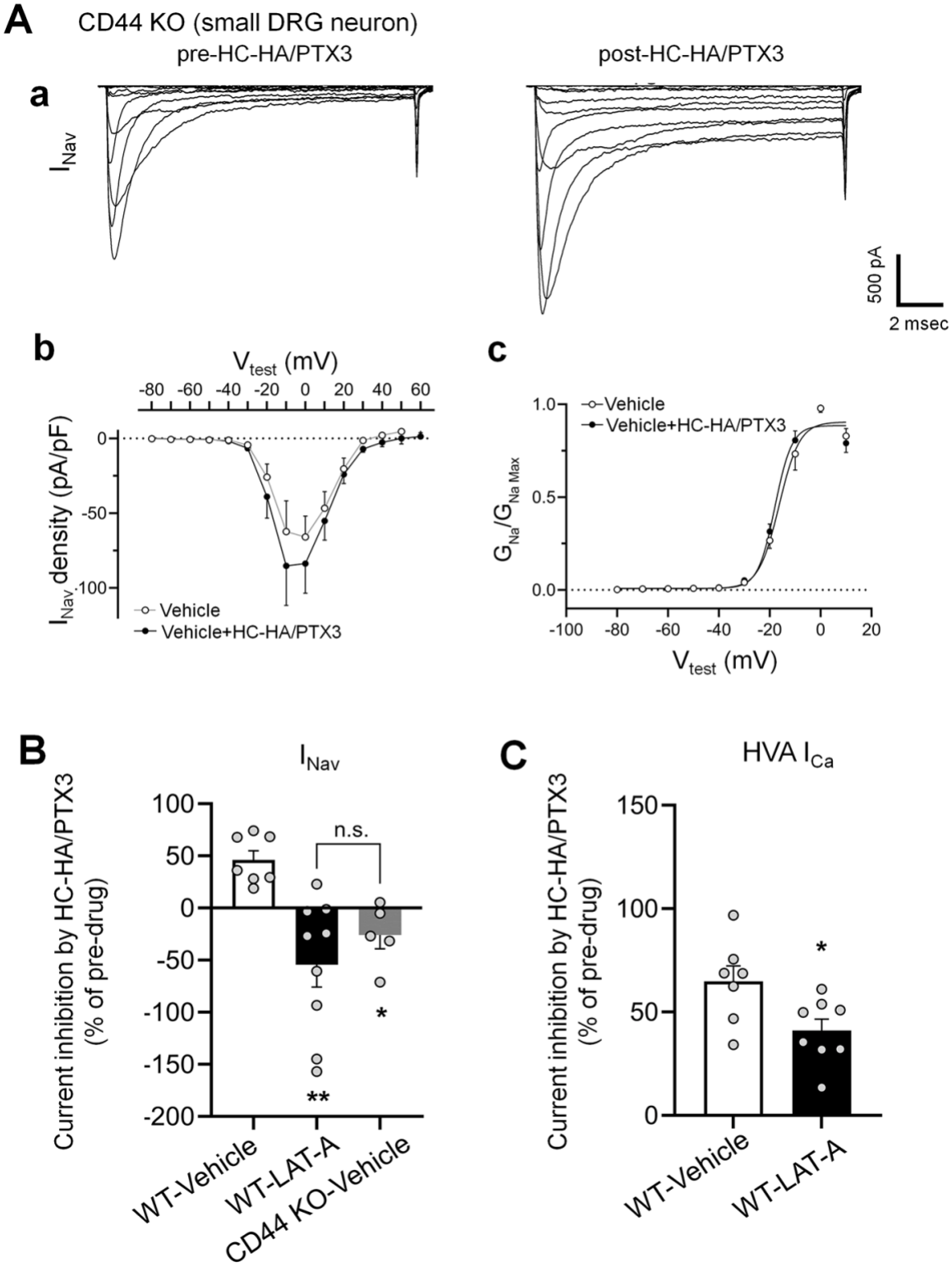

Fig. S7. The inhibitions of I_{Nav} by HC-HA/PTX3 in small-diameter DRG neurons were diminished in CD44 KO mice and were inhibited by a pre-treatment of LAT-A

in neurons from WT mice.

(A) HC-HA/PTX3 (10 μg/mL) did not inhibit I_{Nav} in small-diameter DRG neurons from CD44 KO mice. a. Representative traces of I_{Nav} in a CD44 KO neuron before and at 5 min after bath application of HC-HA/PTX3 (10 μg/mL). b. There was no significant change of I_{Nav} density (pA/pF) before and after HC-HA/PTX3 (10 μg/mL) treatment in CD44 KO neurons. c. HC-HA/PTX3 did not alter G_{Na}/G_{Na} max across the test voltages in CD44 KO neurons. N=5. (B) Changes of I_{Nav} after bath application of HC-HA/PTX3 (10 μg/mL) in vehicle-infused (N=7) and LAT-A-infused small WT DRG neurons ($P<0.01$, N=9), and in vehicle-infused CD44 KO neurons (N=5). DRG neurons were infused with the vehicle or LAT-A (0.5 nM) through the recording electrode, followed by bath application of HC-HA/PTX3 (10 μg/mL) 5 min later. The lumbar DRG neurons were harvested on Days 2-3 after the plantar incision. DRG neurons were categorized according to cell body diameter as <20 μm (small), 20–30 μm (medium), and >30 μm (large). Data are mean ± SEM. One-way ANOVA with Holm-Sidak post-test. $^{*}P < 0.05$, $^{**}P<0.01$ versus WT-vehicle pretreatment group. (C) The inhibition of HVA I_{Ca} by HC-HA/PTX3 (10 μg/mL) in vehicle-infused (N=7) and LAT-A-infused small WT DRG neurons ($P=0.02$, N=8). Data are mean ± SEM. Unpaired Student's t-test.

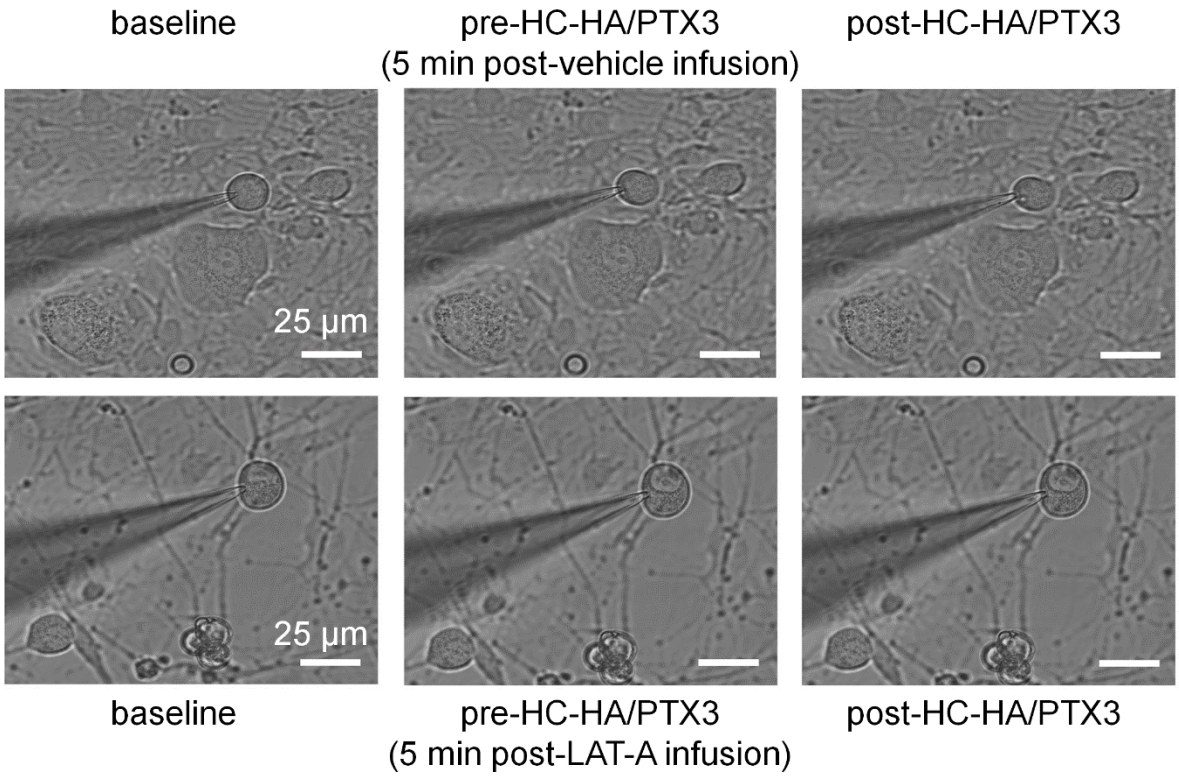

Fig. S8. Intracellular infusion of LAT-A did not change the gross morphology of DRG neurons in patch clamp recordings.
Example images show a small-diameter DRG neuron after infusion vehicle or Latrunculin A (LAT-A, 0.5 nM) through the recording electrode, followed by bath application of HC-HA/PTX3 (15 µg/mL). Scale bar: 25 µm. DRG neurons were categorized according to cell body diameter as <20 µm (small), 20–30 µm (medium), and >30 µm (large).

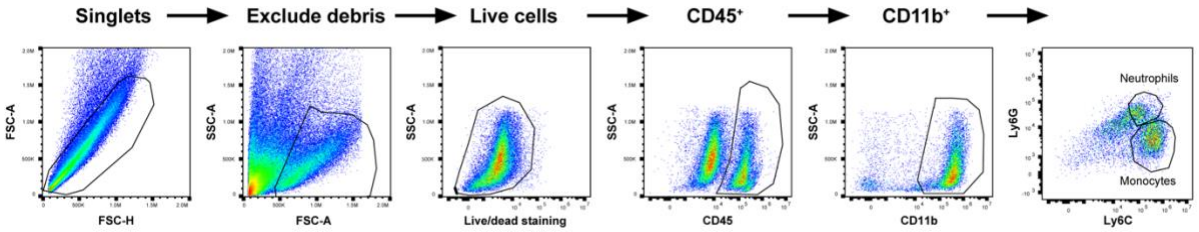

Fig. S9. Representative flow cytometry gating strategy for identification of $CD45^+$ cells, $CD11b^+Ly6G^+$ neutrophils, and $CD11b^+Ly6G^-Ly6C^+$ monocytes in wild-type mice hind paw skin after the plantar-incision.

Table S1. The measures of intrinsic membrane properties of small-diameter DRG neurons in WT and CD44 KO mice.

Knocking out of CD44 did not significantly alter the intrinsic membrane property of DRG neurons, as compared to that in WT mice.

	Wild Type	$CD44^{-/-}$		p-value
V_{rest} (mV)	-49.4 ± 1.4	-48.77 ± 2.1	$t_{(21)} = 0.76$	0.81
Rheobase (pA)	156.9 ± 14.1	154.2 ± 21.81	$t_{(22)} = 0.1$	0.92
AP Threshold (mV)	-32.76 ± 1.29	-31.4 ±1.22	$t_{(22)} = 0.58$	0.57
AP Amplitude (mV)	70.27 ± 4.53	54.55 ± 8.73	$t_{(22)} = 1.69$	0.1
AP50 (msecs)	8.85 ± 0.55	10.02 ± 1.27	$t_{(22)} = 0.98$	0.33
Overshoot (mV)	37.26 ± 4.66	52.8 ± 6.15	$t_{(24)} = 1.69$	0.1
AHP (mV)	-65.47 ± 1.03	-64.05 ± 1.13	$t_{(24)} = 0.71$	0.48
τ-AHP (msecs)	70.98 ± 7.93	56.18 ± 8.63	$t_{(24)} = 0.96$	0.35